Istituto per la Microelettronica e Microsistemi

Consiglio Nazionale delle Ricerche

Emission Mössbauer spectroscopy of topological kagome magnets (INTC-P-687)

Roberto Mantovan[1], Anastasios Markou[2,3], **Edouard Lesne**[3], Claudia Felser[3], Haraldur Pall Gunnlaugsson[4], Hilary Masenda[5], Juliana Schell[6,7], Ian Chang Jie Yap[7], Adeleh Mokhles Gerami[6,8], Carlo Grazianetti[1], and The Mössbauer collaboration at ISOLDE/CERN[9]

[1]***CNR-IMM, Unit of Agrate Brianza (Italy)***, [2]*Department of Physics, University of Ioannina (Greece)*, [3]***Max Planck Institute for Chemical Physics of Solids, Dresden (Germany)***, [4]*Science Institute, Univ. Iceland*, [5]*School of Physics, University of the Witwatersrand (South Africa)*, [6]*European Organization for Nuclear Research (CERN)*, [7]*Institute for Materials Science and Center for Nanointegration Duisburg-Essen (Germany)*, [8]*School of Particles and Accelerators, Institute for Research in Fundamental Sciences (Iran)*, [9]https://e-ms.web.cern.ch/content/collaborators

www.imm.cnr.it

Summary

- Motivation & open questions
- Preliminary results
- Experimental plan to answer open questions

Emission M

Hyperfine Interaction stu

Radioactive probes: ^{57}M

$^{119}In \rightarrow ^{119}Sn$ ($T_{1/2}$ = 2.4 mi

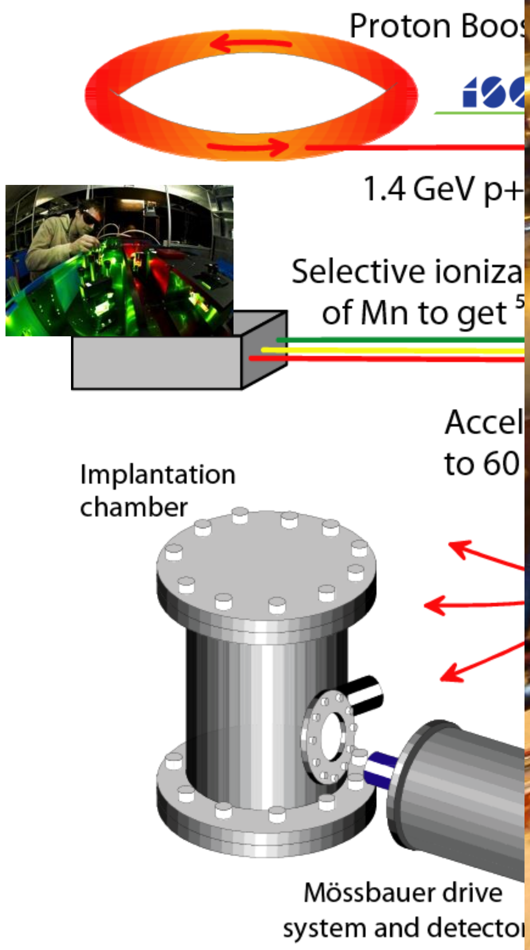

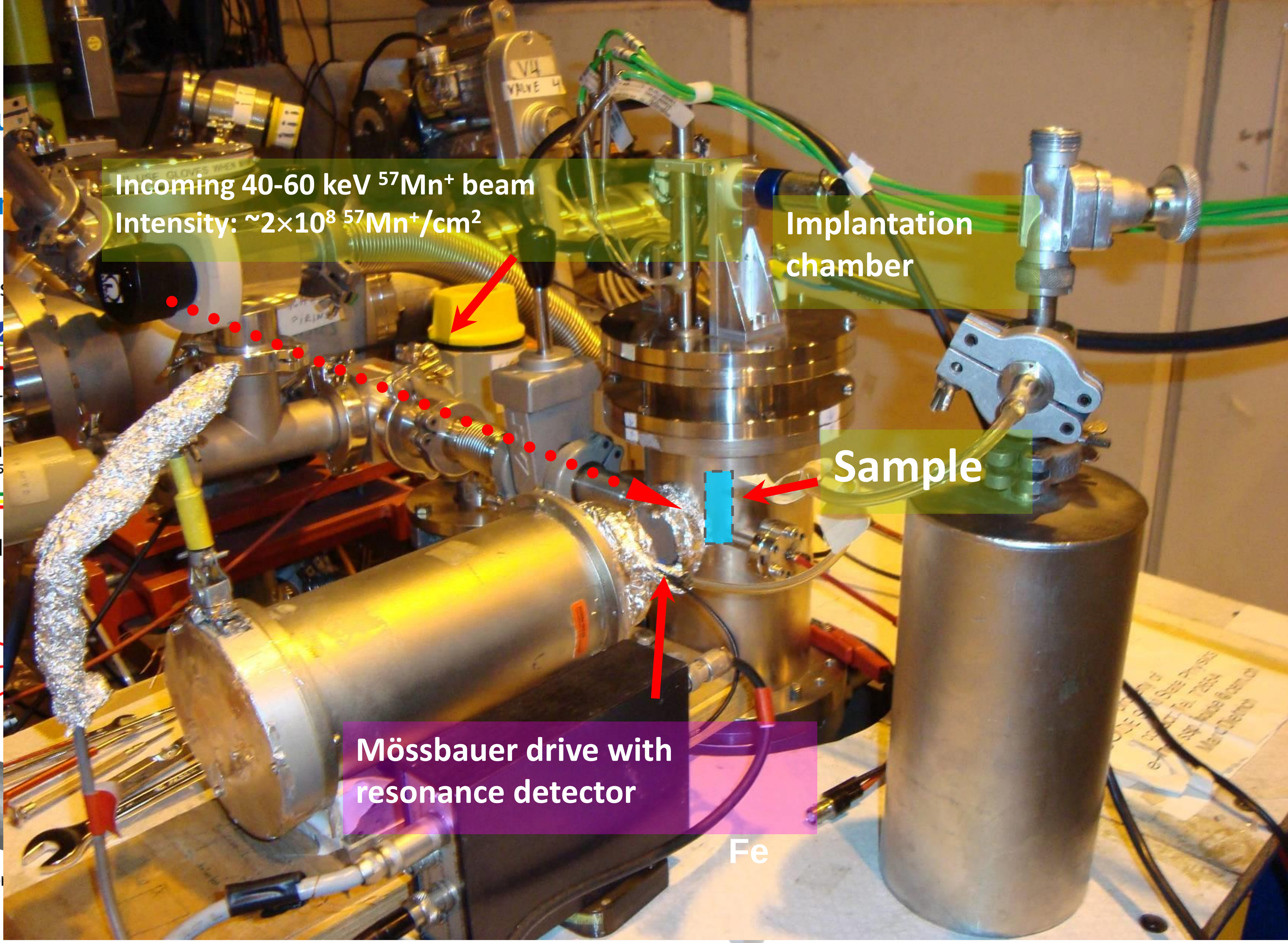

Kagome magnets

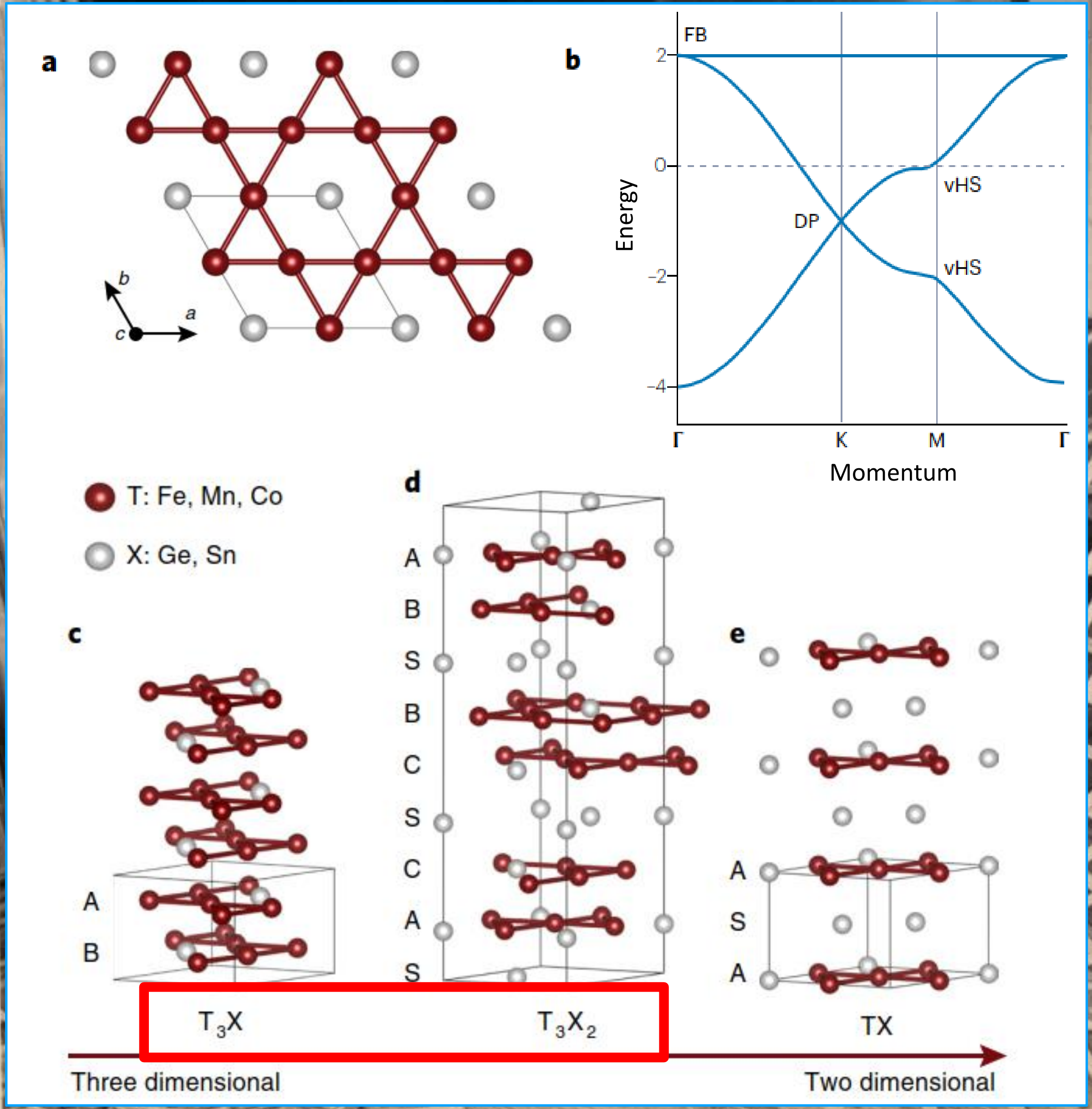

'Kagome' lattice is a **two-dimensional (2D) lattice of corner-sharing triangles**, consisting of 3d transition metal atoms (T: Fe, Mn, Co) with space-filling atoms (X: Sn, Ge) at the centre of the hexagon

Band structure of kagome lattice typically exhibit **Dirac points** (DP) at the K-point, **van Hove singularities** (vHs) at the M-point, and a **flat band** (FB) across the whole Brillouin zone

→ This makes them **intriguing platforms to jointly study and exploit topology, correlated phenomena such as magnetism, and potential instabilities towards long-range many-body orders**

Our interest is in: Fe_3Sn_2, Fe_3Sn, Mn_3Sn

Open issues

Z. Hou et al., Adv. Mater. 29, 1701144 (2017)
K. Heritage et al., Adv. Funct. Mater. 30, 1909163 (2020)

Fe_3Sn_2: Spin-reorientation is thought at the or
formation, as due to T-dependent magnetic anis
atomic-scale view is missing

Fe_3Sn: New rare-earth free permanent magnet
magnetic anisotropy desired). In bulk Fe_3Sn, I
oriented and planar magnetization was observe
…reflecting controversies on the nature of m
anisotropy

Mn_3Sn: Large anomalous Hall effect at RT
Spin-reorientation from in-plane non collinear AFM order to out-of plane spin-spiral structure at 260 K, and transition T is affected by Fe doping (Mn_{3-x}**Fe_x**Sn) **….and atomic-scale view is missing**

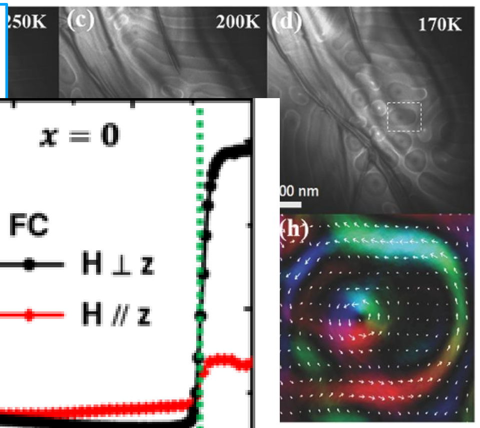

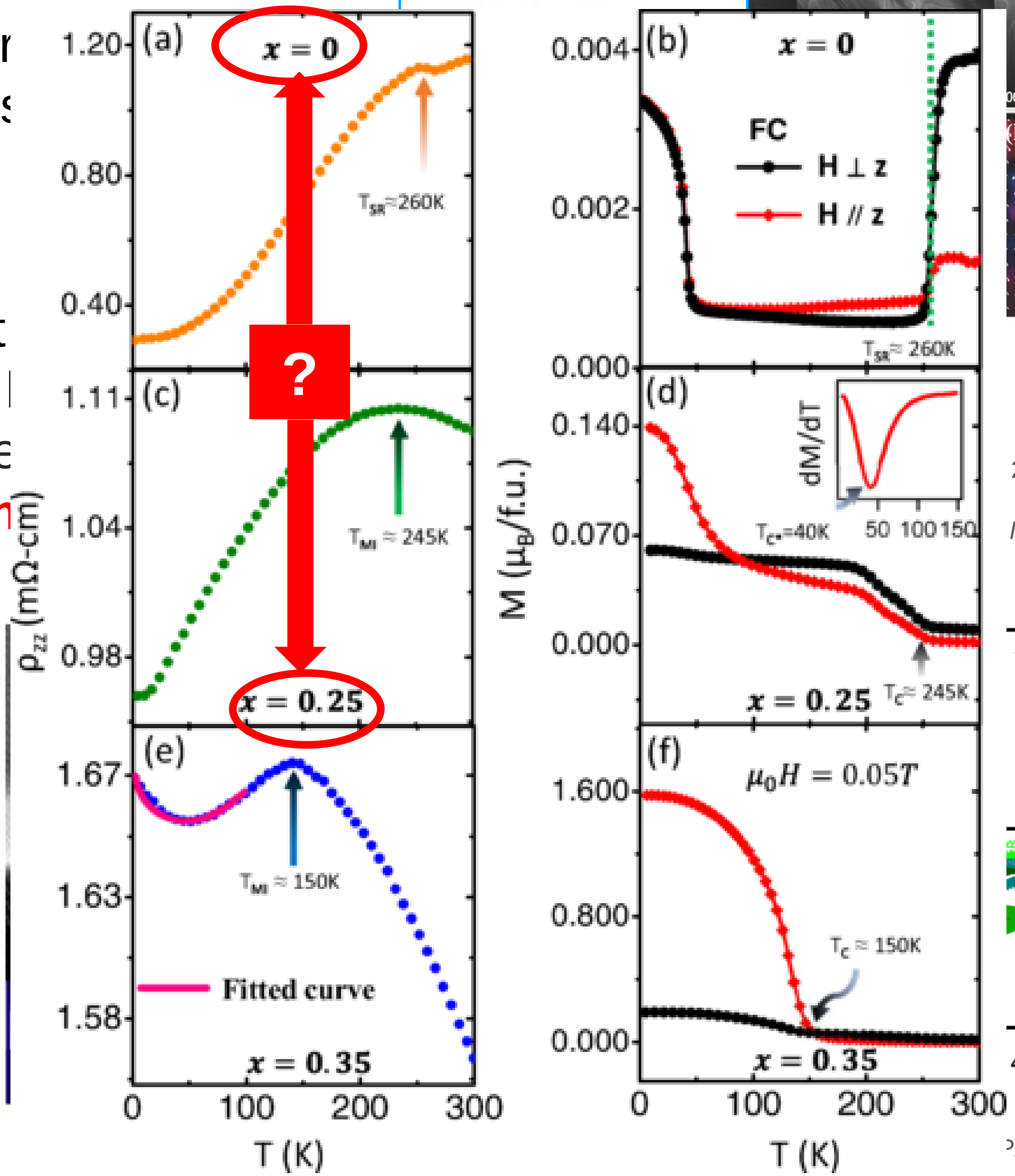

2, 347 (1970)
Rep 4, 7024 (2014)
Interact. 240, 42 (2020)

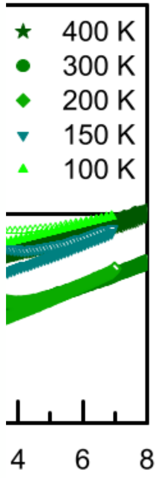

A. Low et al., Phys. Rev. B 106, 144429 (2022)

PRB **101**, 094404 (2020)

Preliminary results

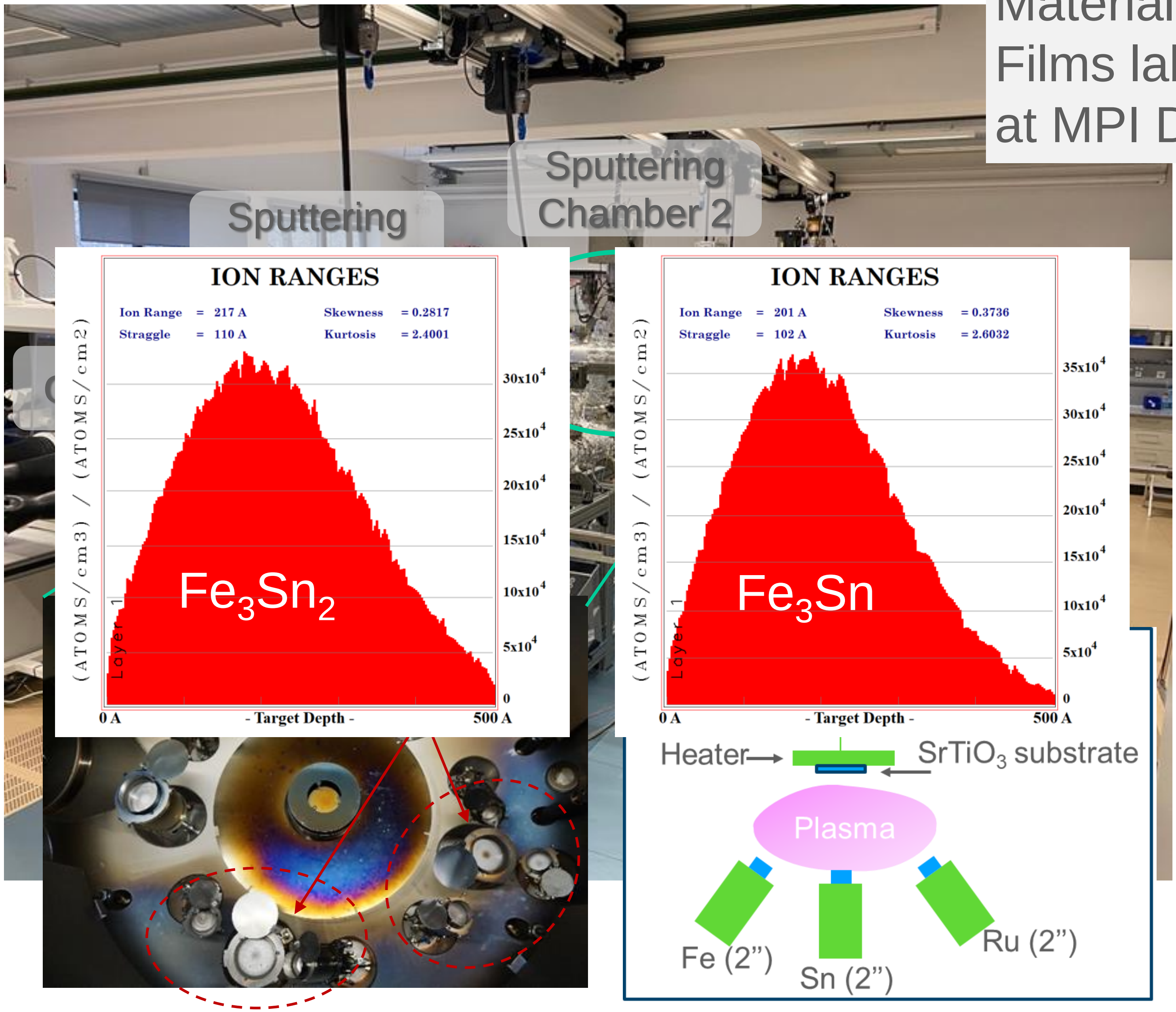

From: Quantum Materials Thin Films laboratory at MPI Dresden

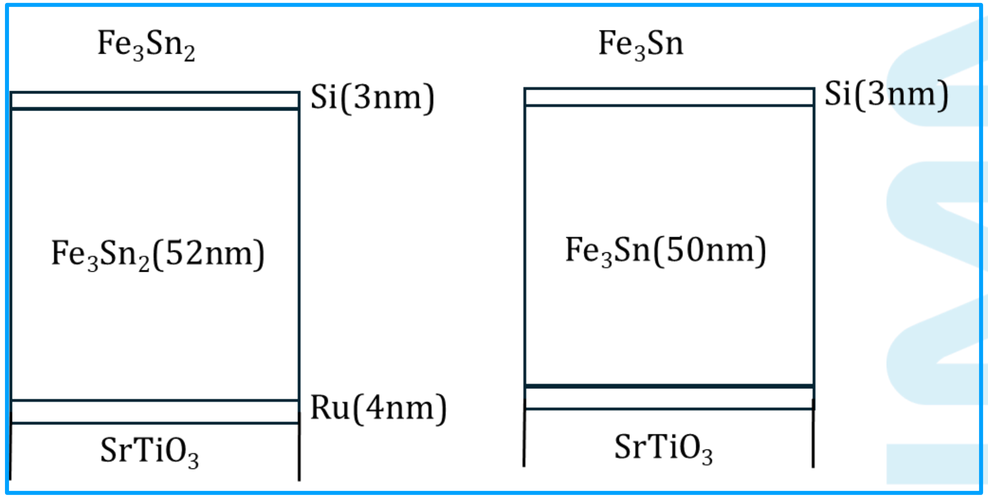

Measured by ^{57}Mn-eMS during the last beamtime in September 2023

Fe_3Sn_2 vs Fe_3Sn (room temperature)

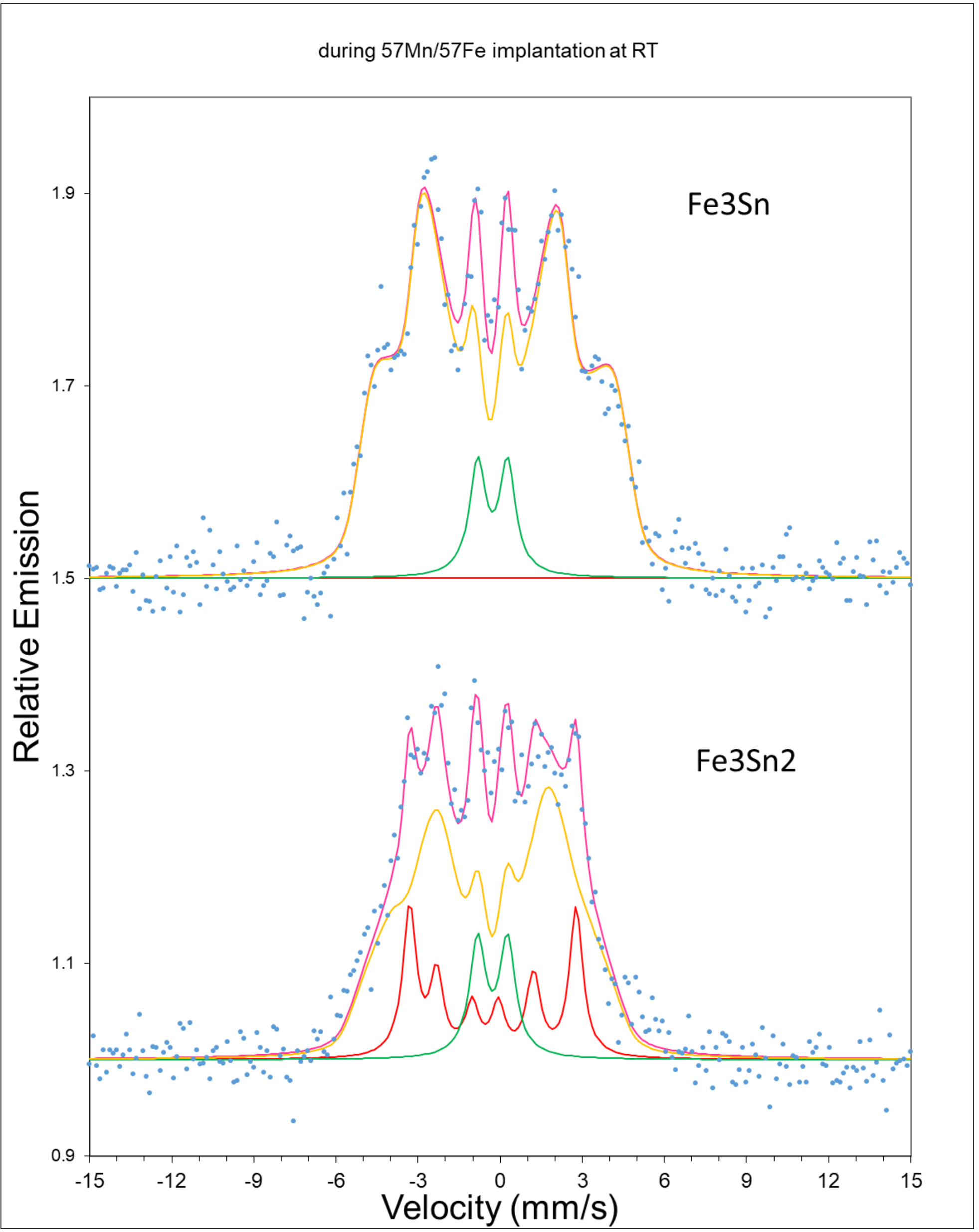

Main observations:

1) The implantation-induced damage does not prevent the **observation of clear magnetic components**

2) ^{57}Mn eMS is **sensitive to stoichiometry** changes at magnetic sites

Fe_3Sn_2 vs Fe_3Sn

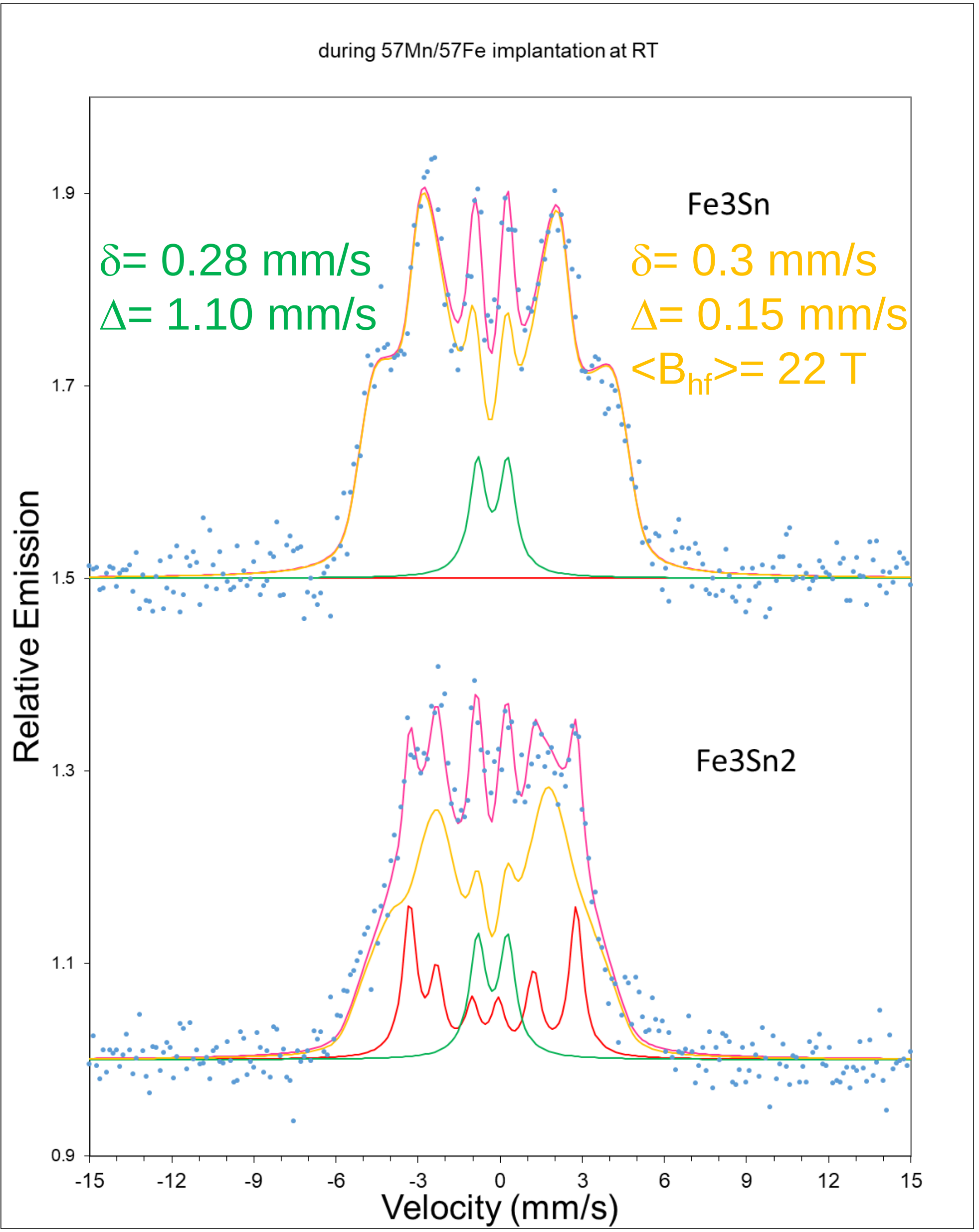

Many MS papers on bulk, very few on films

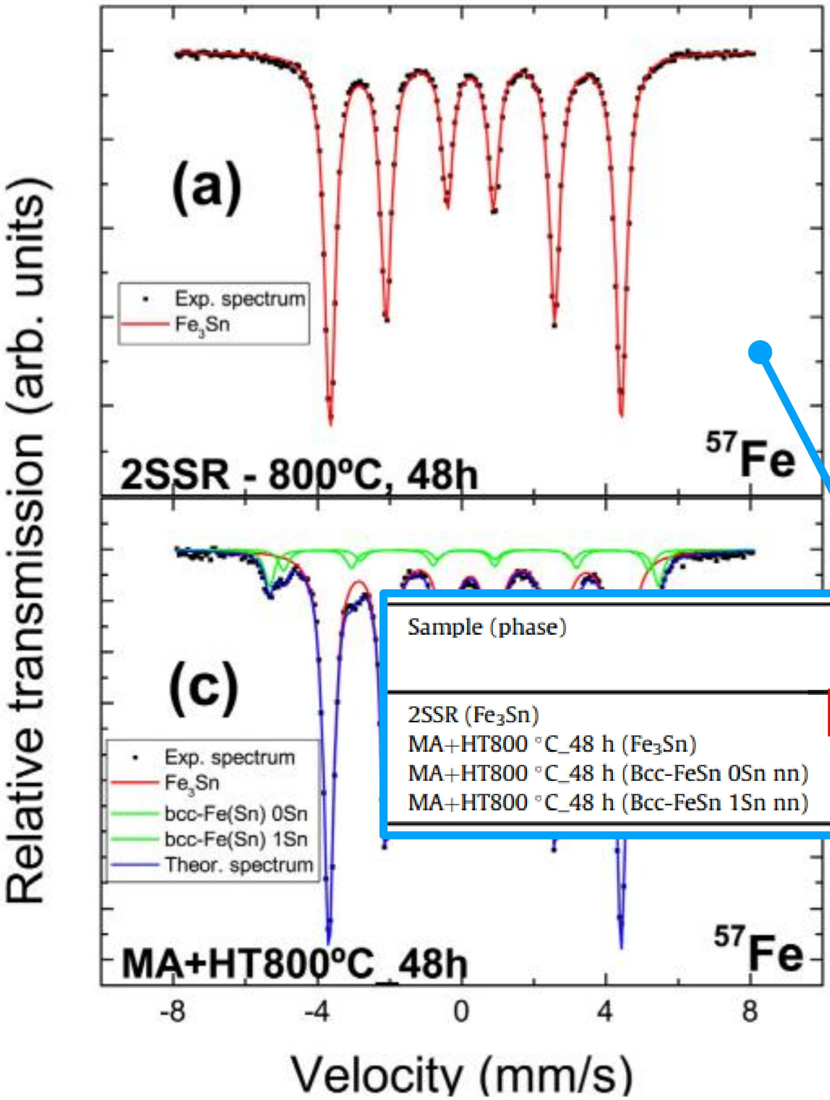

Sample (phase)	^{57}Fe source			
	IS (mm/s)	QS (mm/s)	B_{hf} (T)	Γ (mm/s)
2SSR (Fe_3Sn)	0.30(1)	0.15(1)	25.0(1)	0.37(1)
MA+HT800 °C_48 h (Fe_3Sn)	0.30(1)	0.14(1)	25.1(1)	0.34(1)
MA+HT800 °C_48 h (Bcc-FeSn 0Sn nn)	0.0(1)	0.00(1)	33.3(2)	0.33(1)
MA+HT800 °C_48 h (Bcc-FeSn 1Sn nn)	0.12(1)	0.00(1)	31.4(1)	0.33(1)

Fe_3Sn

Echevarria-Bonet et al, J. All. Comp. (2018)

Also:
Palchucán et al., Hyp. Interact. 241, 42 (2020)

Fe_3Sn_2 vs Fe_3Sn

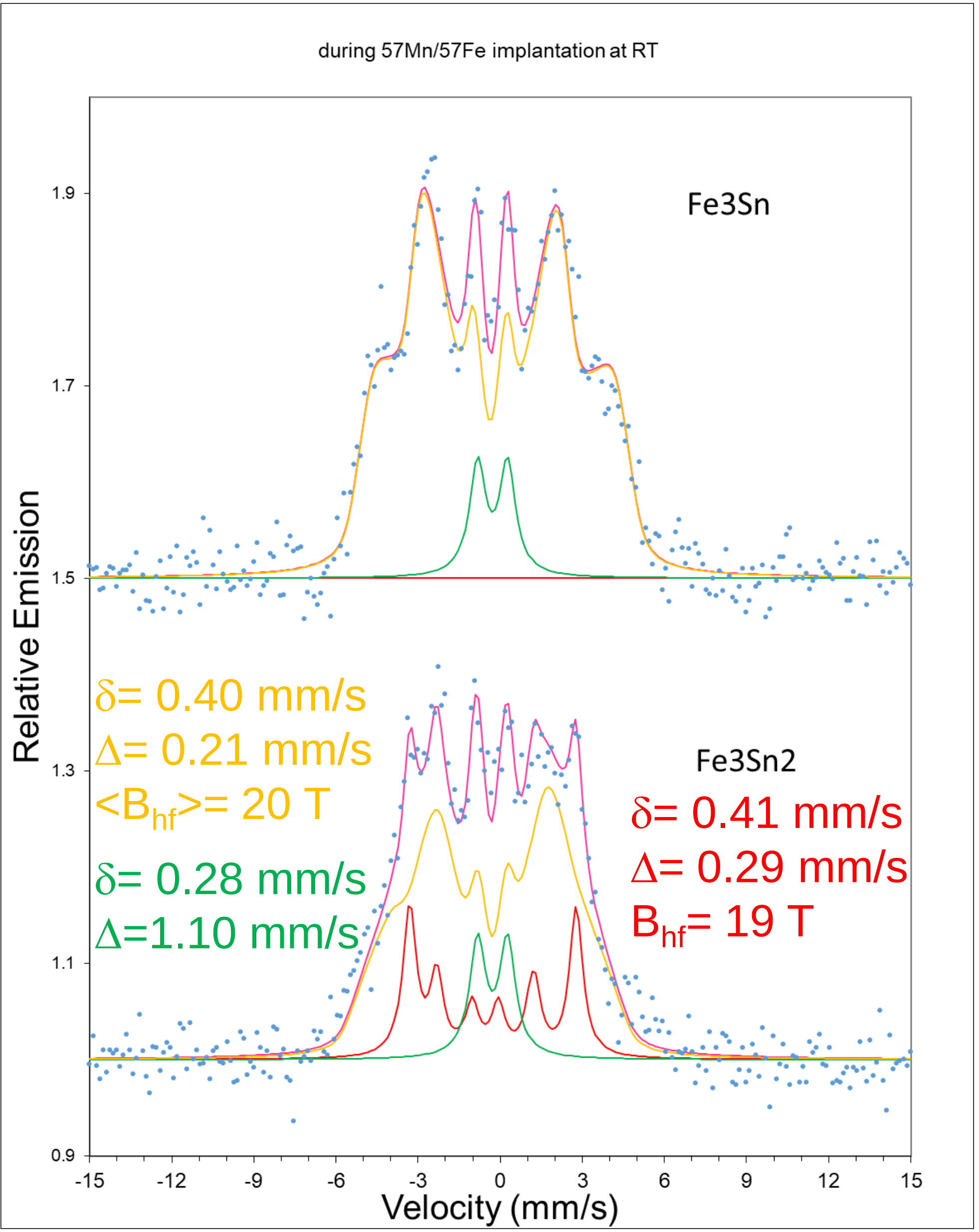

Many MS papers on bulk, very few on films

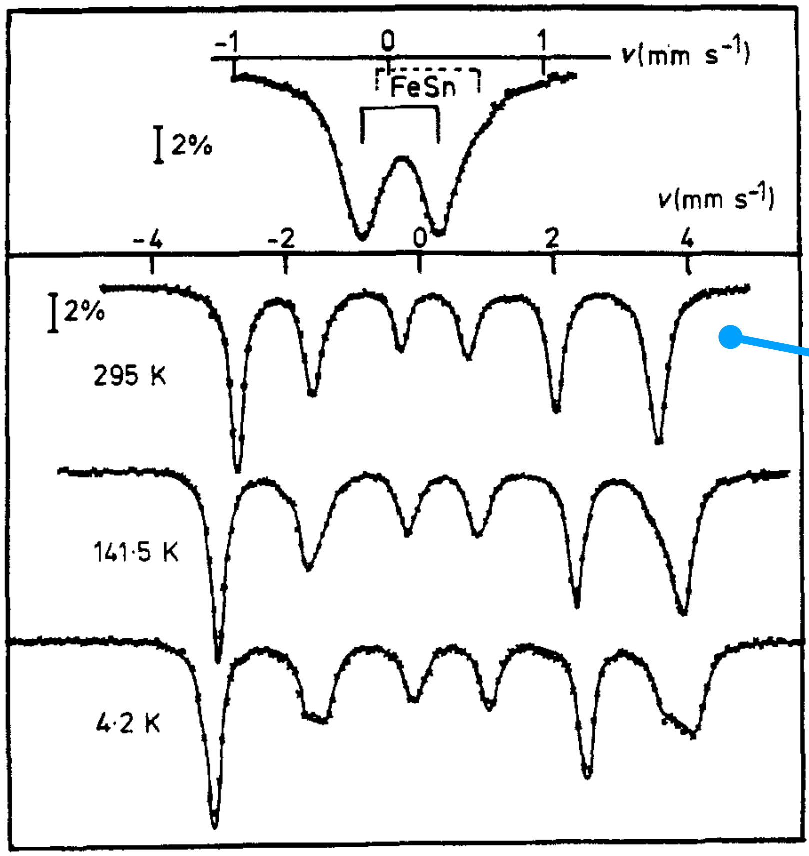

3. Fe_3Sn_2 Structure. Electric field gradient (EFG) tensor

Fe_3Sn_2 belongs to the rhombohedral system, space group $R\bar{3}m$ with $Z = 6$ in a hexagonal unit cell of dimensions $a = b = 5{\cdot}344$ Å, $c = 19{\cdot}845$ Å (Malaman *et al* 1976). This structure can be described as a particular stacking of the hexagonal unit cell of FeSn. This latter unit is repeated in the c direction with a shift $(\frac{2}{3}, \frac{1}{3}, \frac{1}{3})$ and $(\frac{1}{3}, \frac{2}{3}, \frac{2}{3})$ (figure 1).

There is only one crystallographic site for iron in Fe–Sn planes while tin occupies two crystallographically nonequivalent positions: Sn(1) in Fe–Sn planes and Sn(2)

Fe_3Sn_2

G Le Caer et al 1978 J. Phys. F: Met. Phys. 8 323

Table 1. Hyperfine parameters of Fe_3Sn_2 at room temperature

H (kOe)	ϵ ($mm\,s^{-1}$)	δ ($mm\,s^{-1}$)	Γ_1 ($mm\,s^{-1}$)
−200 ±1	0·095 ±0·004	0·330 ±0·005	0·27 ±0·01

Γ_2 ($mm\,s^{-1}$)	Γ_5 ($mm\,s^{-1}$)	Γ_6 ($mm\,s^{-1}$)
0·30 ±0·02	0·25 ±0·01	0·30 ±0·02

Fe_3Sn_2: eMS vs conversion electron-MS (CEMS)

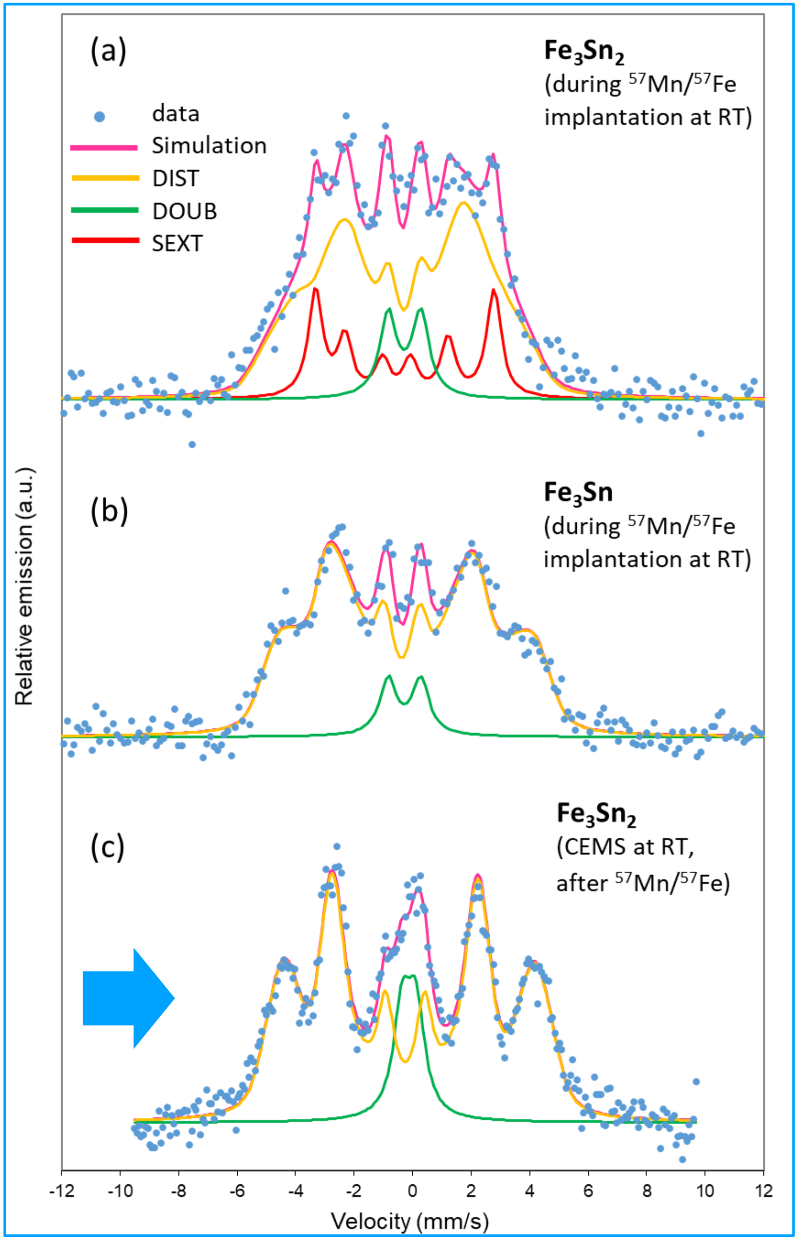

eMS of Fe_3Sn_2 shows additional "sharper" magnetic component

→ From Sn_2 layers?

(…"selective" m gnet c doping of s ane

New open question «born» @ISOLDE

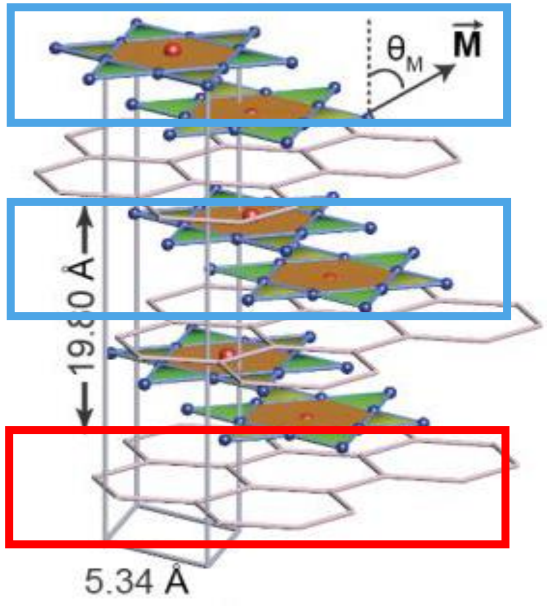

CEMS of Fe_3Sn_2 shows a very similar spectra to eMS of Fe_3Sn

Magnetic stanene?

Tunable electronic and magnetic properties in stanene by 3d transition metal atoms absorption

Dan-Xu Xing, Ceng-Ceng Ren, Shu-Feng Zhang, Yong Feng, Xin-Lian Chen, Chang-Wen Zhang, Pei-Ji Wang*

School of Physics, University of Jinan, Jinan 250022, People's Republic of China

Theoretical paper (2017) **without experimental follow-up**

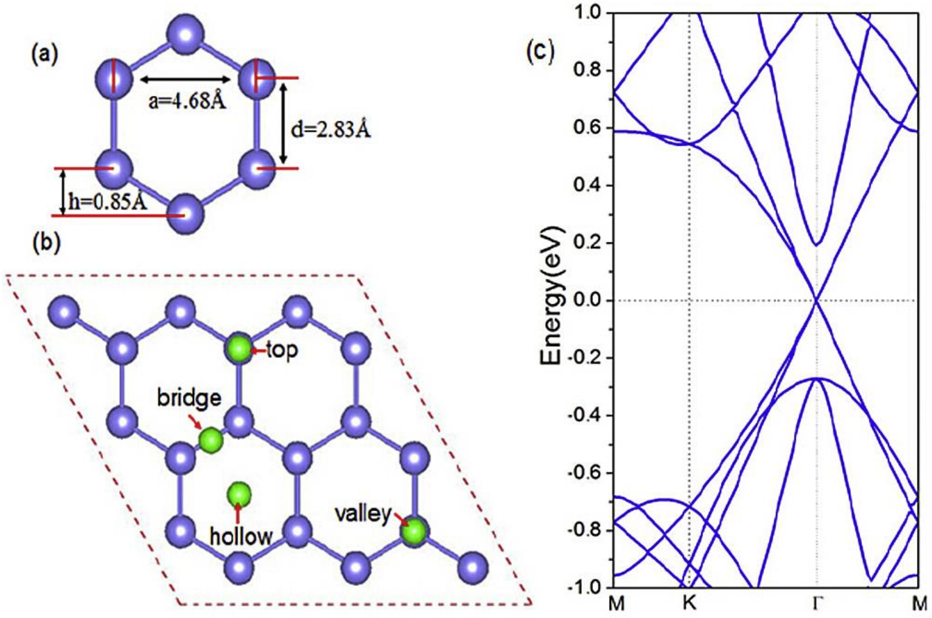

Fe-doping

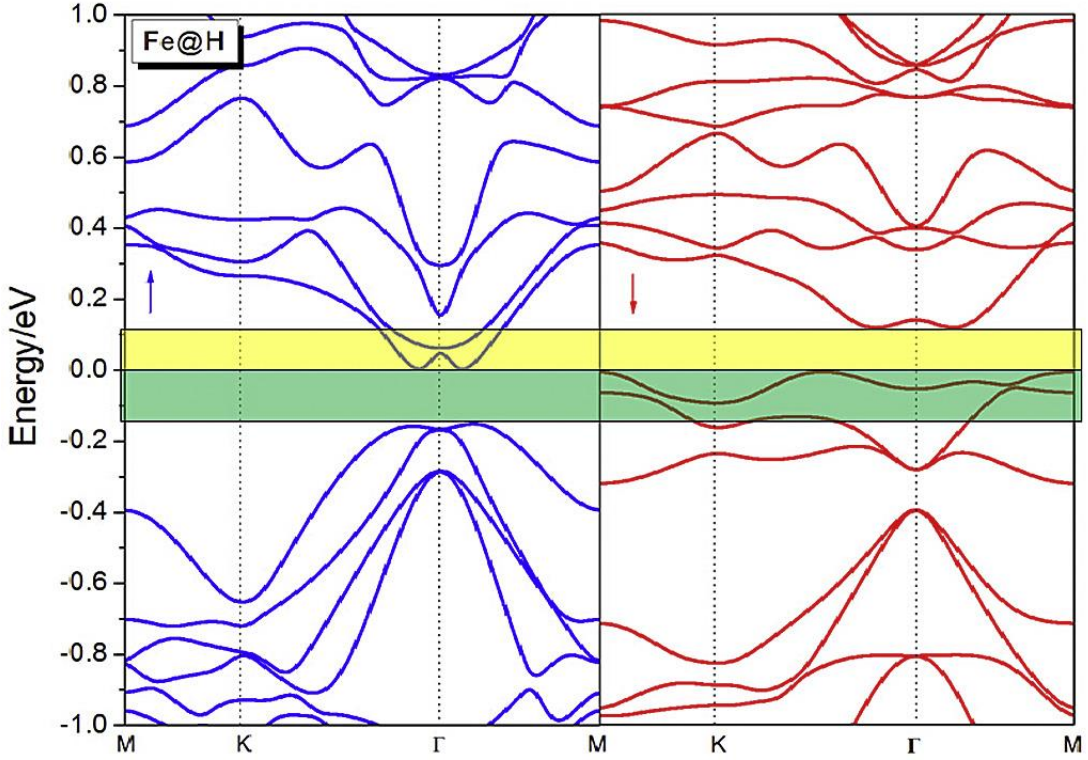

Fe-absorbed stanene is a **bipolar magnetic gapless semiconductor** with up-spin electron and down spin hole carriers to support the coexistence of the charge current and the pure spin current.

Spin polarization induced by Fe at «hollow» sites

D.-X. Xing et al., Superlattices and Microstructures 103 (2017) 139e144

Experimental plan

System to be studied (thickness in parentheses)	*number of samples*	*hours with HT-lid*	*hours with LT-lid*	*hours with ROT-lid*
substrate/buffer(Ru, ≤4nm)/**Fe_3Sn_2** (≥50nm)/capping(≤3nm), sputtering	≥2 (at least 2 thicknesses)	5	4	6
substrate/buffer(Ru, Pt ≤4nm)/**Fe_3Sn** (≥50nm)/capping(≤3nm), sputtering	≥2 (at least 1 per each buffer)	5	4	6
substrate/buffer(Ru ≤4nm)/**Mn_3Sn** (≥50nm)/capping(≤3nm), sputtering	≥2 (at least 2 thicknesses)	5	4	6
substrate/buffer(Ru, Pt ≤4nm)/**Fe_3Sn_2**/capping, MBE	≥2 (at least 2 thicknesses or buffer)	5	4	6

HT-lid: eMS up to 600-700 K → full characterization of atomic-scale magnetism up to the Curie temperature. To carefully follow (and compare) the evolution of the DIST and SEXT components in Fe_3Sn_2 and Fe_3Sn will be fundamental to **get insight into the nature of SEXT observed in Fe_3Sn_2**

LT-lid: eMS down to ~100 K → follow the hyperfine magnetic field evolution at low T to explore the **atomic-scale origin of spin reorientation processes**

ROT-lid: eMS at variable angles, with or without an applied magnetic field of ~ 0.6 T → determine the **nature of magnetic interactions**, to study the **magnetic anisotropies**, and to determine **site symmetry** of paramagnetic doublets

Experimental plan

System to be studied (thickness in parentheses)	*number of samples*	*hours with HT-lid*	*hours with LT-lid*	*hours with ROT-lid*
substrate/buffer(Ru, ≤4nm)/**Fe_3Sn_2** (≥50nm)/capping(≤3nm), sputtering	≥2 (at least 2 thicknesses)	5	4	6
substrate/buffer(Ru, Pt ≤4nm)/**Fe_3Sn** (≥50nm)/capping(≤3nm), sputtering	≥2 (at least 1 per each buffer)	5	4	6
substrate/buffer(Ru ≤4nm)/**Mn_3Sn** (≥50nm)/capping(≤3nm), sputtering	≥2 (at least 2 thicknesses)	5	4	6
substrate/buffer(Ru, Pt ≤4nm)/**Fe_3Sn_2**/capping, MBE	≥2 (at least 2 thicknesses or buffer)	5	4	6

Fe_3Sn: probe the **role of buffer layers (Ru, Pt)** in stabilizing different strain states, i.e. Fe_3Sn is expected to be compressively strained by -1.2% *vs* tensely strained by + 0.85%, when grown on Pt *vs* Ru buffer layers respectively

We plan thickness in the range of 30 ÷ 100 nm. Thicker layers will experience strain relaxation towards their bulk lattice parameters, while intermediate thicknesses will likely show some strain gradient. From TRIM: we're mostly sensitive to the first 20÷30 nm closer to the surface → by comparing experiments in samples of ~ 30 nm and > 80 nm → **we'll probe the influence of structural distortions on the hyperfine parameters**, an information hardly accessible by CEMS, as did previously for Fe/V superlattices [*T. E. Mølholt et al., Crystals 12, 961 (2022)*]

Final objective is to answer open questions:

- Can we induce **magnetic ordering in Sn_2-stanene** layers in Fe_3Sn_2?
- What is the atomic-scale origin of **spin reorientation** in Fe_3Sn_2 thin films?
- What is the atomic-scale origin of the **magnetic anisotropy** in Fe_3Sn and Mn_3Sn?
- What is the effect of dilute Fe-doping on the **magnetic anisotropy** in Mn_3Sn?
- What is the **effect of kagome's dimensionality** (i.e. thickness) on their electronic and magnetic properties?

Request: 9 shifts of ^{57}Mn + 2 shifts of ^{119}In

Extra slides

Emission Mössbauer spectroscopy @ISOLDE/CERN

A unique method to investigate **atomic-scale chemical-structural-magnetic properties of materials** in ultra-dilute implantation regime (10^{-3}÷10^{-5} at.%)

Fe defects in Si, Ge, SiGe,…

1998-2005

Dilute magnetism in oxides, semiconductors

2005-2015

Wider range of interests

>50 research papers have been published
https://e-ms.web.cern.ch/content/publications

From 2014… ***several new groups worldwide got interested in eMS and joined the team → new materials, new ideas, new collaborations...***

Fe_3Sn_2

(top) Top view of an individual Fe_3Sn layer with kagome structure
(bottom) Sn_2 layer with honeycomb structure ("stanene")

Side view of the crystal structure of Fe_3Sn_2 consisting of alternating stacking of two Fe_3Sn kagome layers and one Sn_2 layer

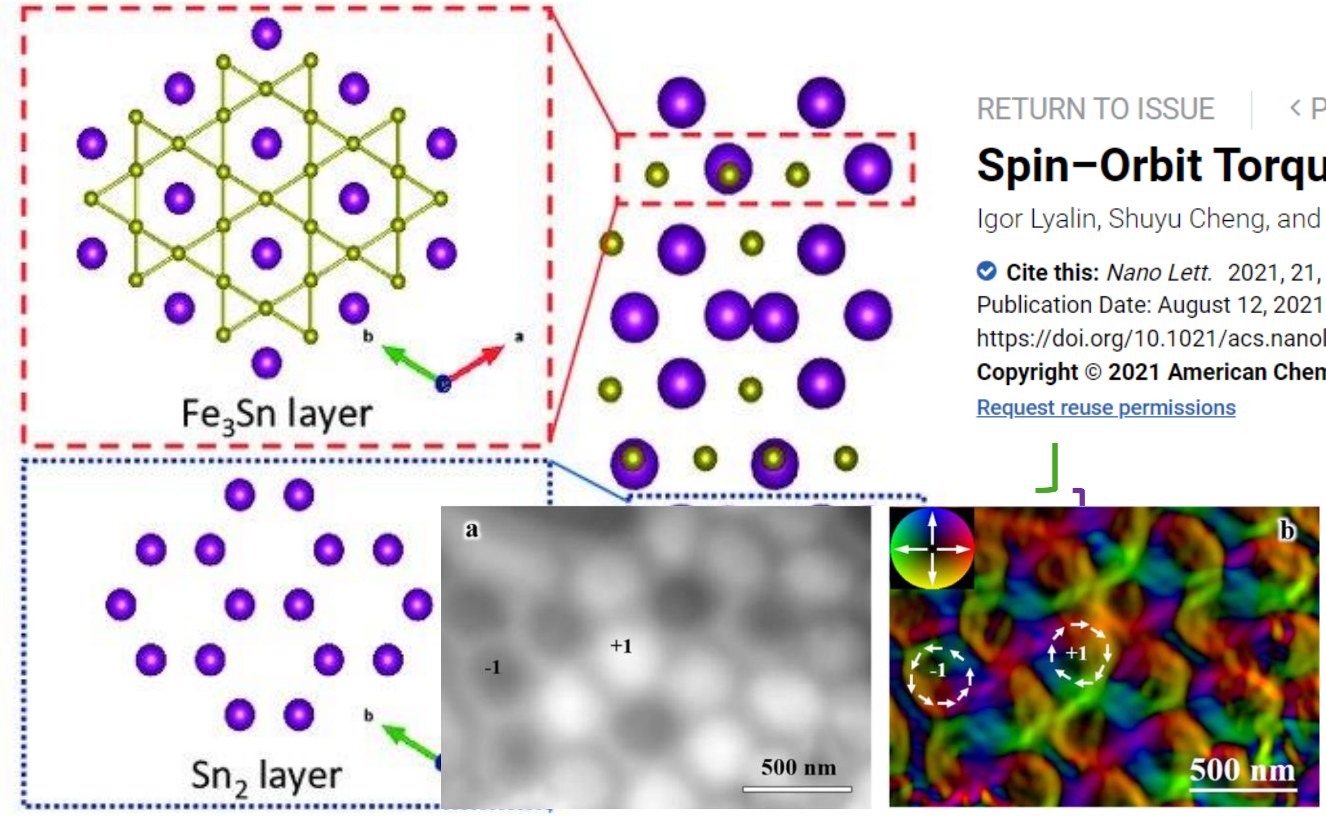

https://arxiv.org/abs/2105.12203

Article | Open access | Published: 15 November 2022

Plethora of tunable Weyl fermions in kagome magnet Fe_3Sn_2 thin films

Zheng Ren, Hor
Bahrami, Fazel Taft

npj Quantum Mate

Issue 23, 2022

Previous Article Next Article

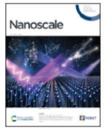

From the journal:
Nanoscale

Intrinsic anomalous Hall effect in thin films of topological kagome ferromagnet Fe_3Sn_2†

Check for updates

RETURN TO ISSUE < PREV **LETTER** NEXT >

Spin–Orbit Torque in Bilayers of Kagome Ferromagnet Fe_3Sn_2 and Pt

Igor Lyalin, Shuyu Cheng, and Roland K. Kawakami*

Cite this: *Nano Lett.* 2021, 21, 16, 6975–6982
Publication Date: August 12, 2021
https://doi.org/10.1021/acs.nanolett.1c02270
Copyright © 2021 American Chemical Society
Request reuse permissions

Article Views 2741 | Altmetric - | Citations 5
LEARN ABOUT THESE METRICS

Share Add to Export
RIS

ADVANCED QUANTUM TECHNOLOGIES

Full Paper | Open Access

Room-Temperature Skyrmion Thermopower in Fe_3Sn_2

Qianheng Du, Myung-Geun Han, Yu Liu, Weijun Ren, Yimei Zhu, Cedomir Petrovic

First published: 11 September 2020 | https://doi.org/10.1002/qute.202000058 | Citations: 10

Fe_3Sn_2 open issues

LTEM images of the magnetic domain structures:

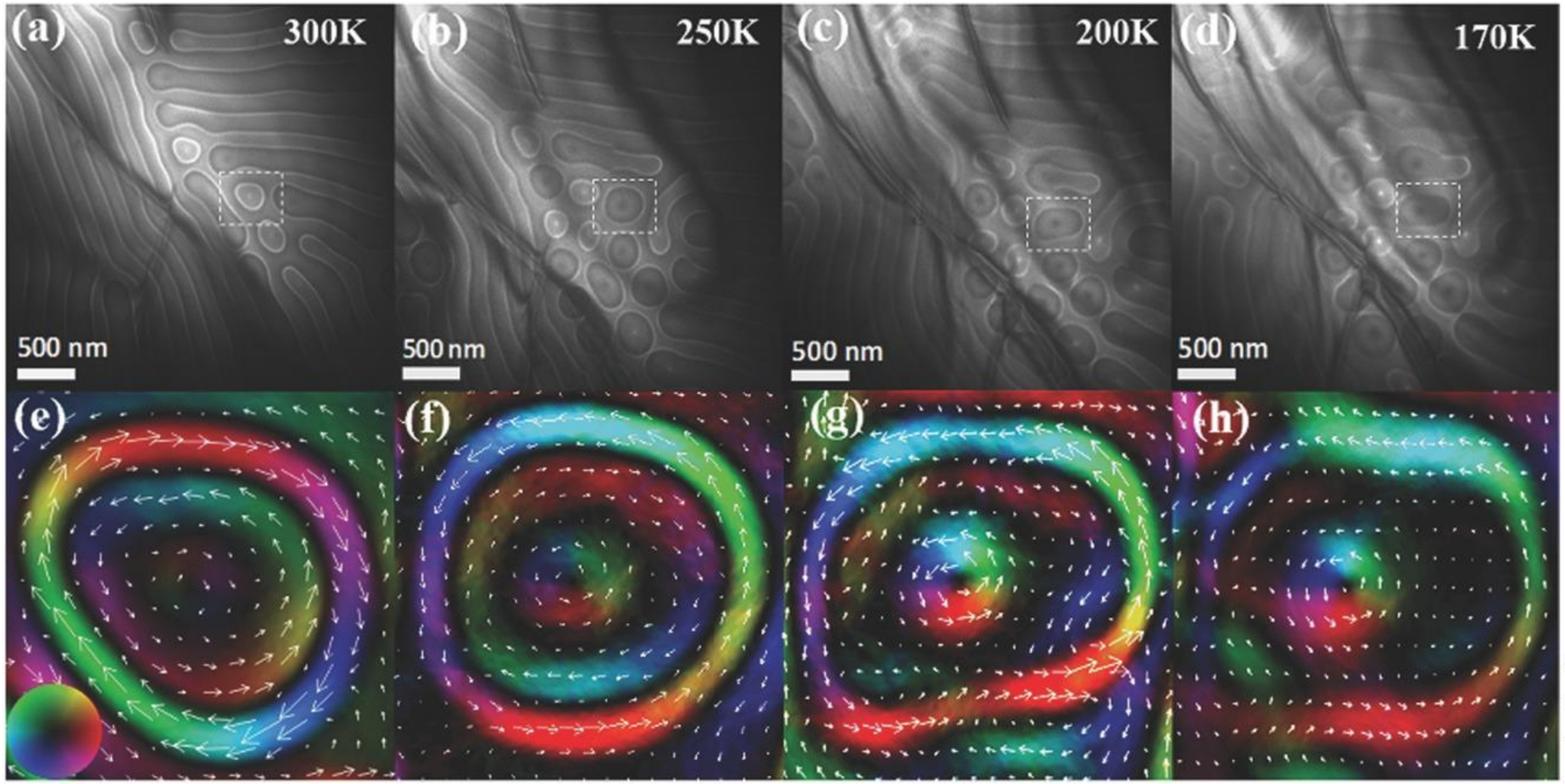

Stripe domains and skyrmionic bubbles coexist in the sample over the temperature range of 300 to 170 K, after turning off the magnetic field.

Spontaneous skyrmionic bubbles with triple-ring structures and random helicities are observed.

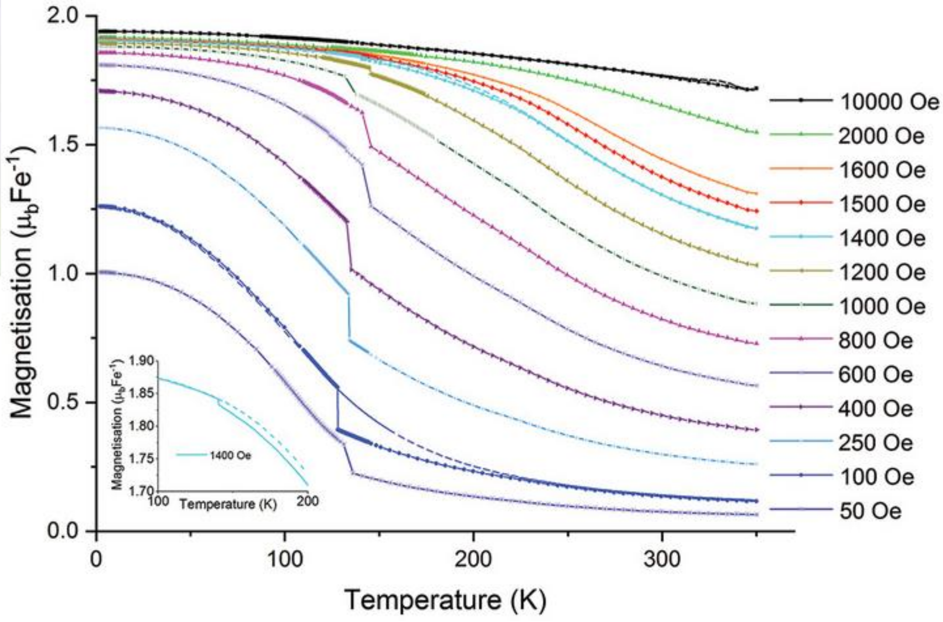

Spin-reorientation is thought at the origin of skyrmion formation, as due to T-dependent magnetic anisotropy

… an atomic-scale view of spin-reorientation in Fe_3Sn_2 films is missing

Z. Hou et al., Adv. Mater. 29, 1701144 (2017)
K. Heritage et al., Adv. Funct. Mater. 30, 1909163 (2020)

Fe_3Sn open issues

Interest as novel rare-earth free permanent magnet
→ Planar magnetocrystalline anisotropy is undesirable

- From Mössbauer studies on bulk Fe_3Sn, *G. Trumpy et al.* [*PRB 2, 347 (1970)*] claimed that the existence of a single sextet proves the magnetization is directed along the c-axis

- Direct magnetic measurements indicate the existence of planar anisotropy [*B. C. Sales et al., Sci. Rep 4, 7024 (2014)*]

There is a certain controversy on the nature of the Fe_3Sn magnetic anisotropy

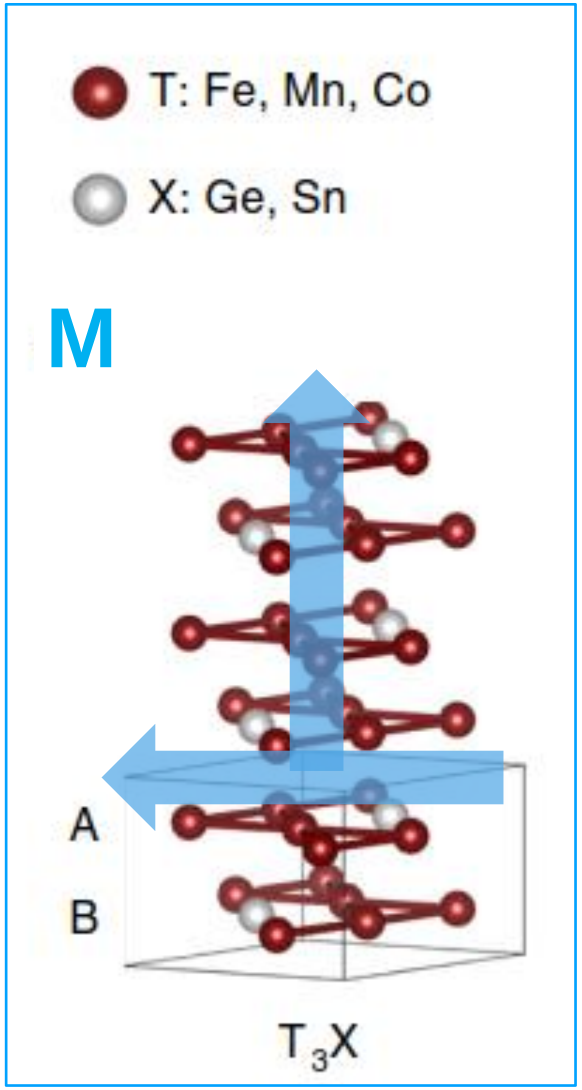

Palchucan et al, Hyp. Interact. 240, 42 (2020)

Mn_3Sn open issues

Hexagonal antiferromagnet

Large anomalous Hall effect observed

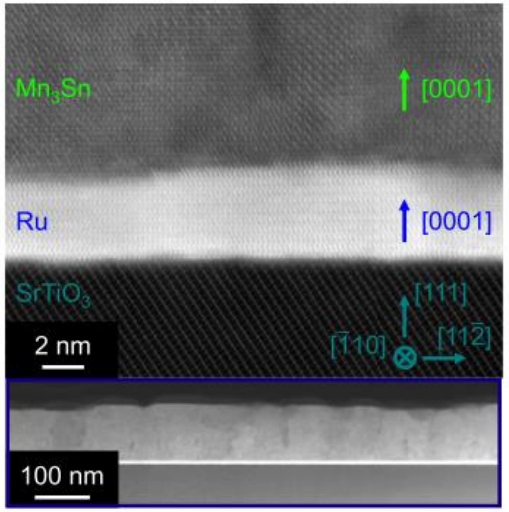

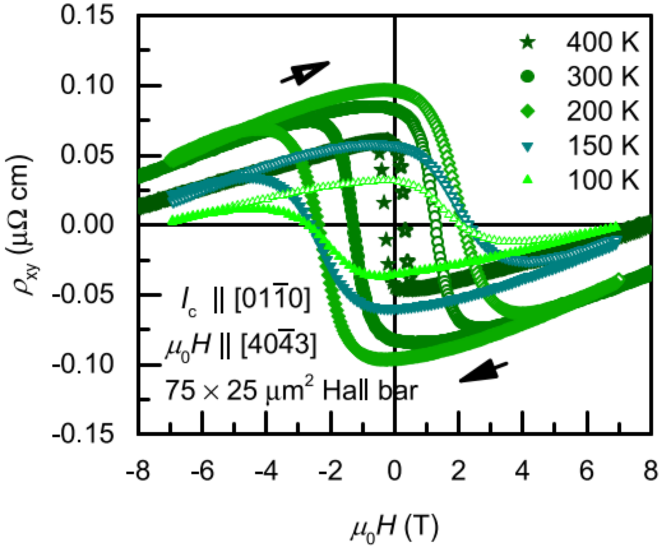

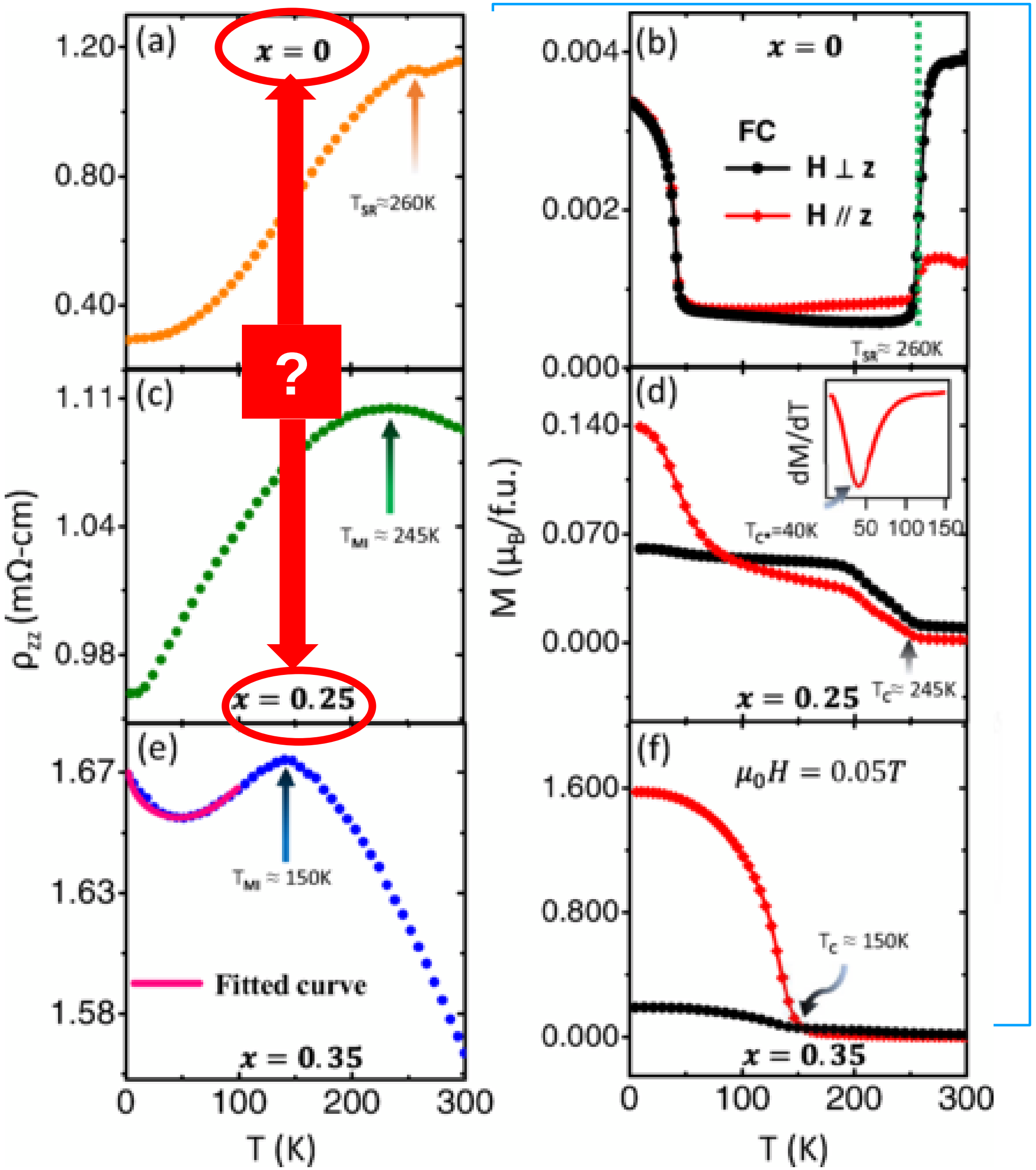

Mn_3Sn is found to show a spin-reorientation **from in-plane non collinear AFM order to out-of plane spin-spiral structure** at 260 K

In **$Mn_{3-x}Fe_xSn$** the spin-reorientation transition temperature shifts

Insight into the atomic-scale view of spin-reorientation? + role of Fe-doping?

A. Low et al., Phys. Rev. B 106, 144429 (2022)

Complementary studies (before and after eMS)

- **SQUID and/or VSM** to measure macroscopic magnetic properties
- **X-Ray Diffraction and X-Ray Reflectivity** to ensure about the crystalline quality and the epitaxial relationships of the layers, as well as to accurately verify their thickness
- **CEMS** → the comparison among (i) CEMS before eMS, (ii) eMS, and (iii) CEMS after eMS, will provide the most comprehensive atomic-scale study that can be done in these kagome magnets
- **DFT simulations** will be used to calculate electric field gradient and electron density of Fe and Sn in Fe_3Sn_2, Fe_3Sn, and Mn_3Sn, focusing on various Fe and Sn sites and configurations of defect complexes around them, in order to univocally determine the nature of the observed magnetic components

Growth of Fe_3Sn_2 and Fe_3Sn epitaxial films

Sputtering chamber

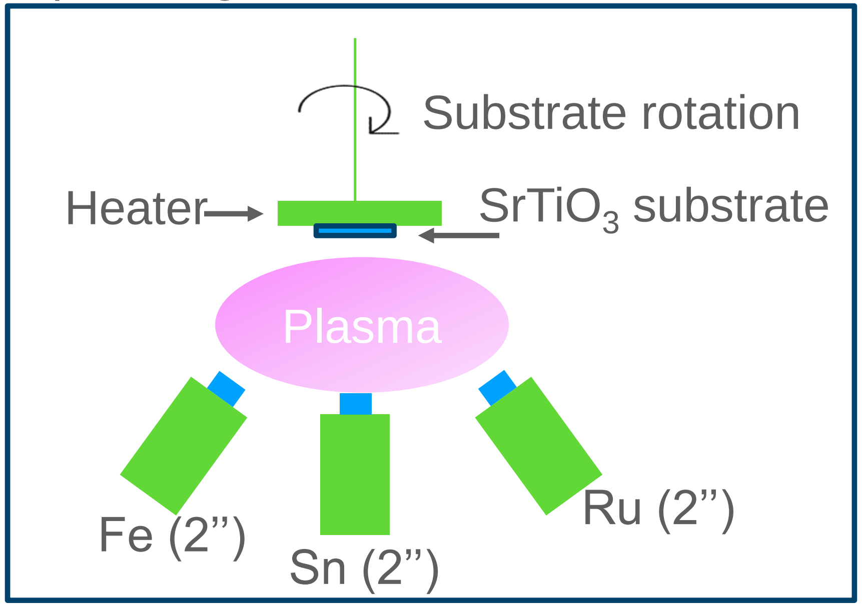

- High temperature growth of a 4 nm–thick Ru seed layer on the $SrTiO_3$ substrate.
- Growth of either 50 nm – thick Fe_3Sn_2 and Fe_3Sn epilayers by keeping constant the Sn- power and adjusting the Fe-power.
- Finally, growth of a Si capping layer to prevent oxidation of the films.

Fe_ySn_x heterostructures

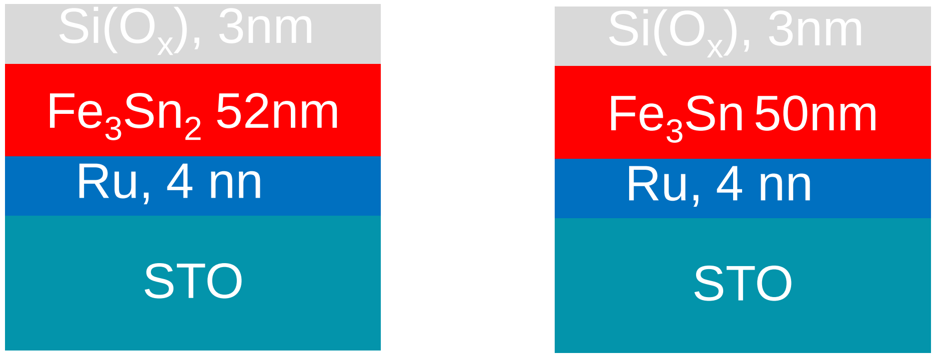

Fe_3Sn_2, Fe_3Sn: XRD & AFM

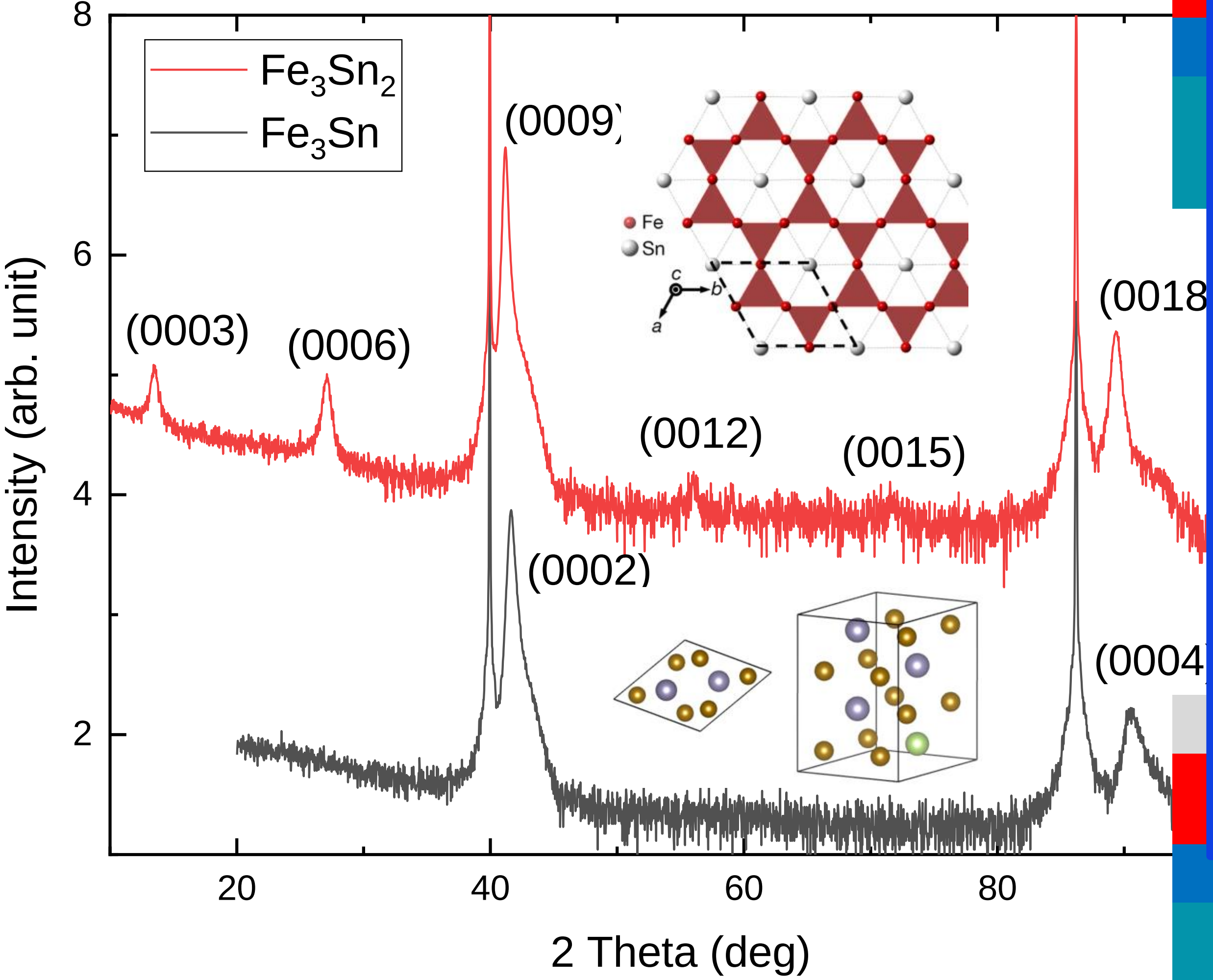

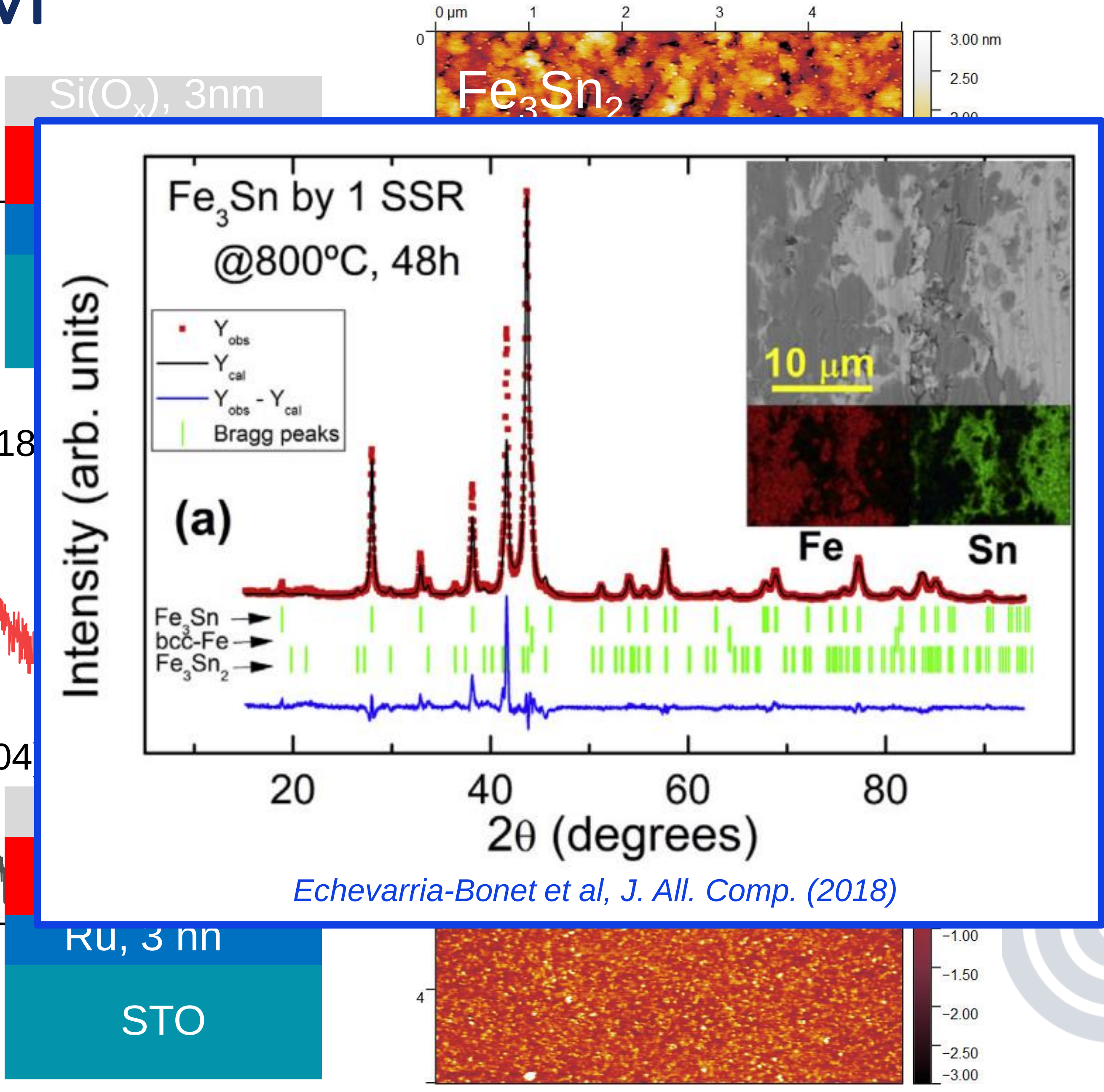

Echevarria-Bonet et al, J. All. Comp. (2018)

MBE of Fe_3Sn_2 @CNR-IMM, Unit of Agrate Brianza

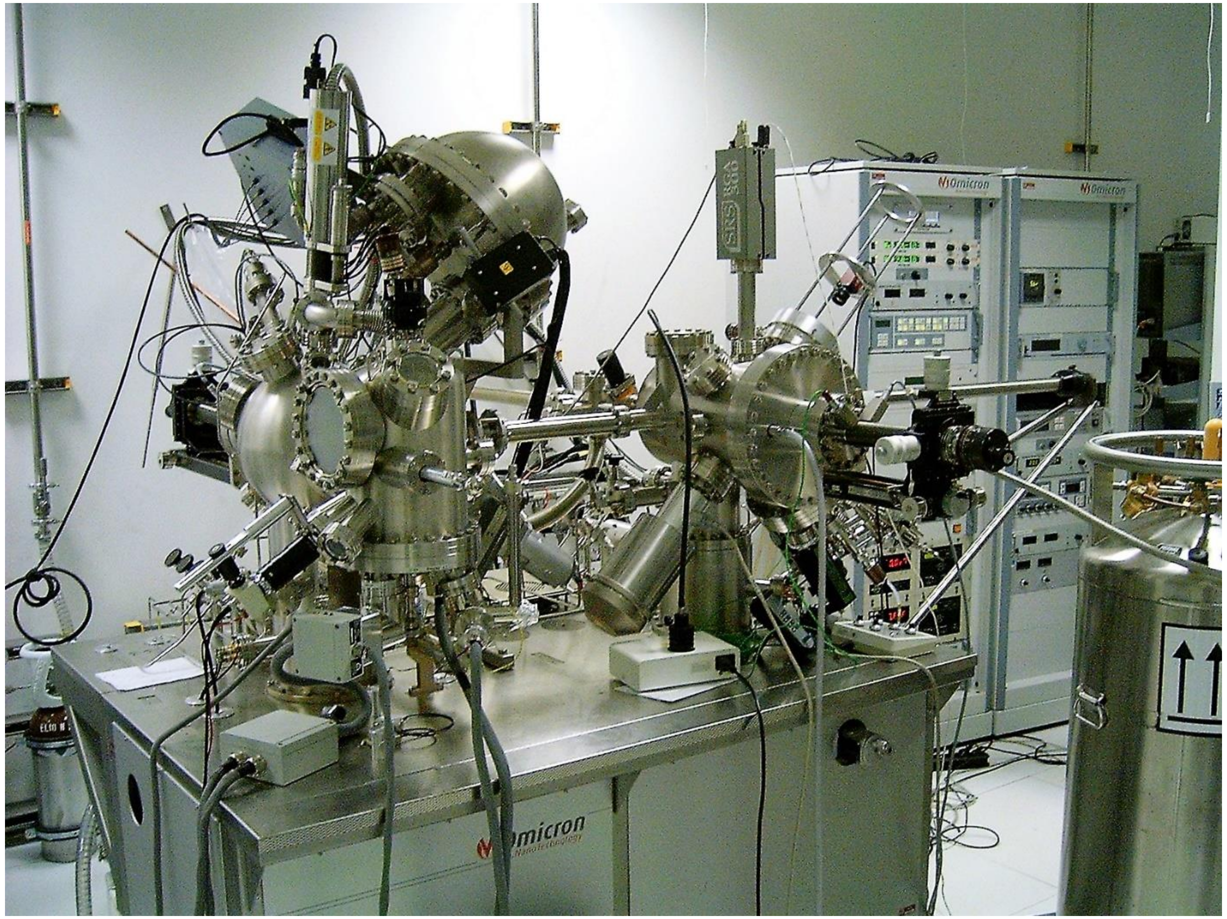

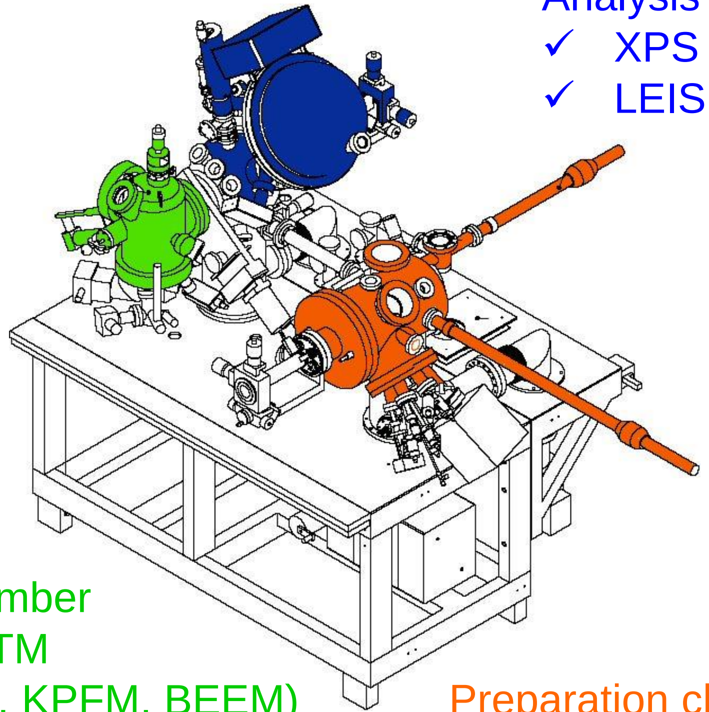

Analysis chamber
- ✓ XPS
- ✓ LEIS

SPM chamber
- ✓ VT-STM
- ✓ (AFM, KPFM, BEEM)

Preparation chamber
- ✓ MBE e-beam evaporators
- ✓ K-cell
- ✓ Atomic gas (O_2,N_2,H_2) source
- ✓ RHEED
- ✓ RGA
- ✓ Thickness monitor

- Interest in using **Fe_3Sn_2 for quantum computations**
- High technological interest to compare Fe_3Sn_2 as produced with two different thin film depositions' methods

NQSTI
National Quantum Science and Technology Institute

PNRR MUR project
PE0000023-**NQSTI**
(2022-2025) https://nqsti.it/

Table of the stopping ranges of 57Mn at 50 keV

Material	Mean	Standard Deviation	Skewness	Kurtosis
Fe_3Sn_2	21.7 nm	11.0 nm	0.2817	2.4001
Fe_3Sn	20.1 nm	10.2 nm	0.3736	2.6032
Mn_3Sn	21.9 nm	10.9 nm	0.2728	2.4103

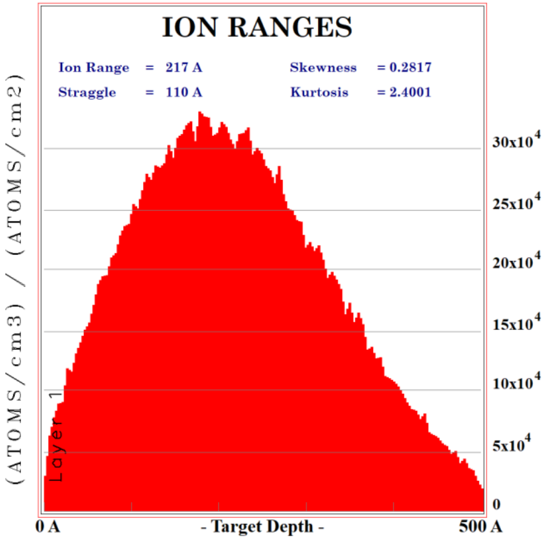

Fe_3Sn_2

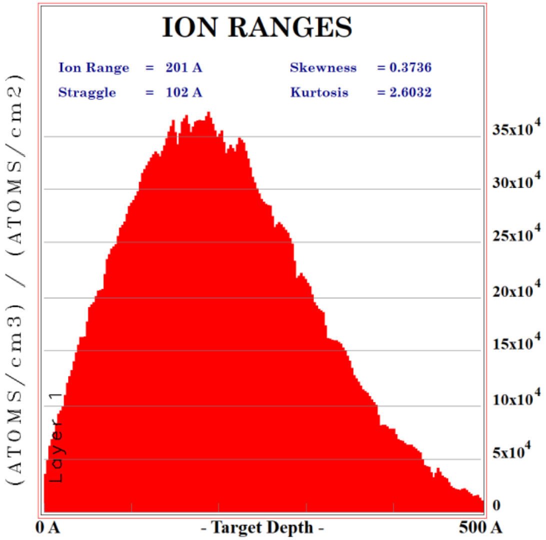

Fe_3Sn

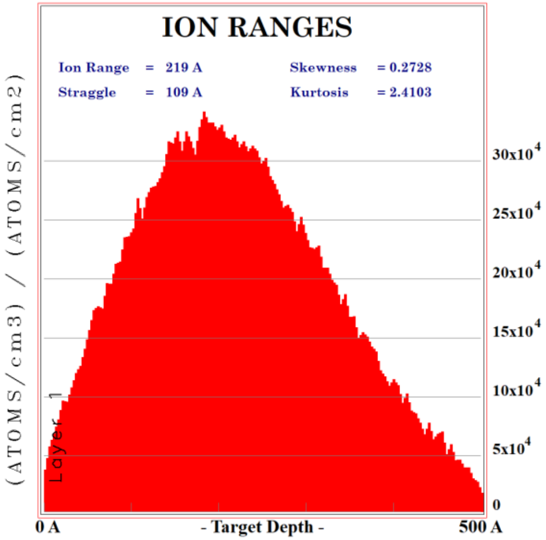

Mn_3Sn

Table of the stopping ranges of 57Mn at 30 keV

Material	Mean	Standard Deviation	Skewness	Kurtosis
Fe_3Sn_2	14.8 nm	8.0 nm	0.5839	3.1096
Fe_3Sn	13.4 nm	7.1 nm	0.5710	3.1533
Mn_3Sn	14.8 nm	7.9 nm	0.5793	3.1555

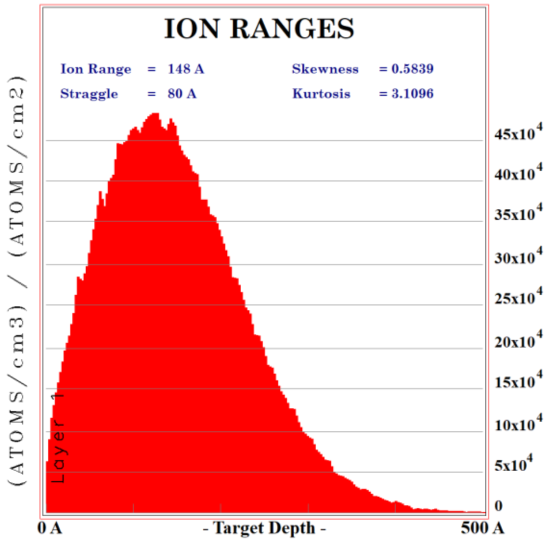

Fe_3Sn_2

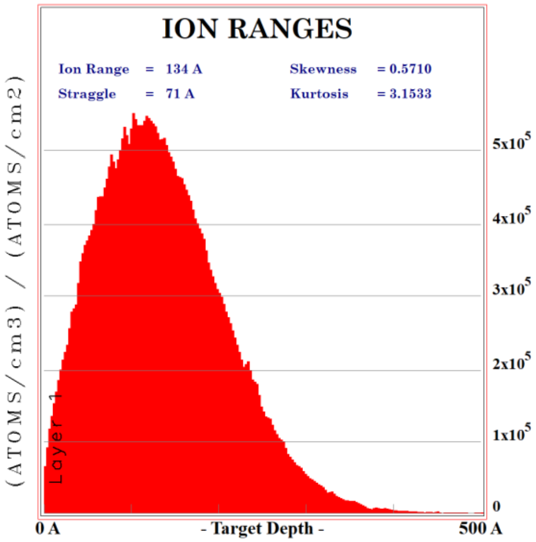

Fe_3Sn

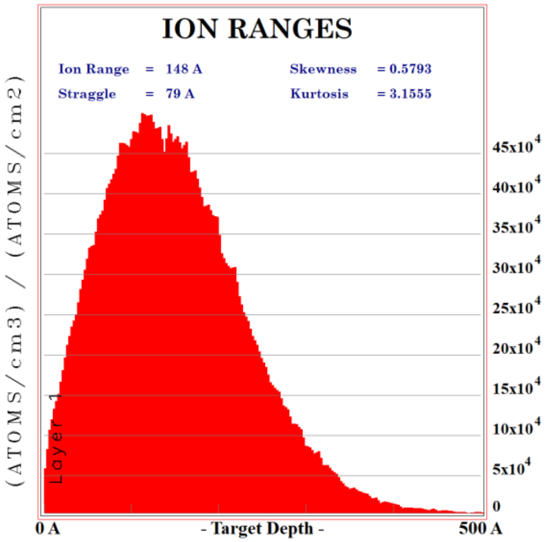

Mn_3Sn

Hyperfine parameters (room temperature)

		iso (mm/s)	*qua (mm/s)*	*<B$_{hf}$>(T)*	*<Γ> (mm/s)*	*A$_{25}$*	*%*
Fe_3Sn_2 (a)	DIST	0.39553818	0.212423061	19.8584242	0.6	2.680403	69.76329
eMS	DOUB	0.283737105	1.10484316	-	0.71363211	-	9.992749
	SEXT	0.413563814	0.285084558	18.8771655	0.6	1.622843	20.24396
Fe_3Sn (b)	DIST	0.3	0.15	21.9428538	0.6	2.684257	91.49941
eMS	DOUB	0.283737105	1.10484316	-		-	8.50059
	SEXT	-	-	-	-	-	0
Fe_3Sn_2 (c)	DIST	-0.188106369	0.143022715	25.1408391	0.60786706	3.150171	86.20511
CEMS	DOUB	0.120992088	0.474187244	-	0.71363211	-	13.79489
	SEXT	-	-	-	-	-	0

Sample TMS1456 (Fe_3Sn_2)

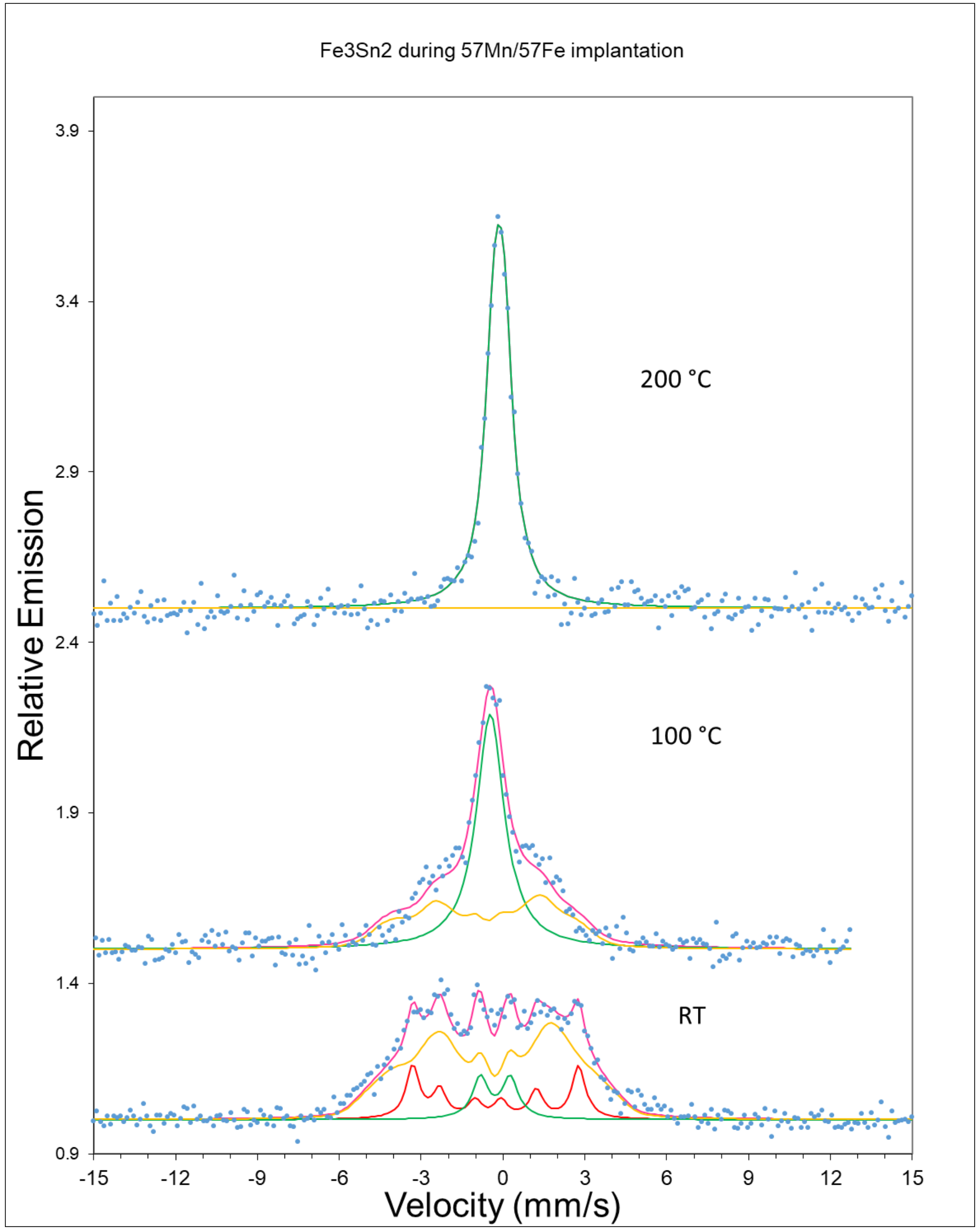

SexGenS		DBL		DIST2			
						B (T)	*f* (relative)
B_{hf} (T)	18.877165			δ_0 (mm/s)	-0.3955382	33	0
δ (mm/s)	-0.4135638	δ (mm/s)	-0.2837371	δ_1 (mm/s/T)	0	27.560502	-1.9422947
ΔE_Q (mm/s)	0.2850846	ΔE_Q (mm/s)	1.1048432	$\Delta E_{Q,0}$ (mm/s)	-0.2124231	21	-3.7762395
		Γ (mm/s)	0.7136321	$\Delta E_{Q,1}$ (mm/s	0	5	0
Outer/middle/inner							
Γ (mm/s)	Area ratio			Γ_{16} (mm/s)	0.6		
0.6	3			Γ_{25} (mm/s)	0.6		
0.6	**1.6228433**			Γ_{34} (mm/s)	0.6		
0.6	1			A_{16}	3		
				A_{25}	2.6804029		
				A_{34}	1		
				Nb	3		
				Average B			
				19.858424			
				Standard dev.			
				5.7973243			
Area (%)	20.243965	Area (%)	9.9927486	Area (%)	69.763287		

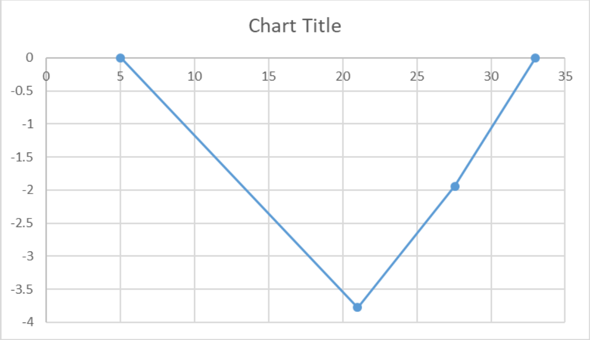

Sample TMS1437 (Fe_3Sn)

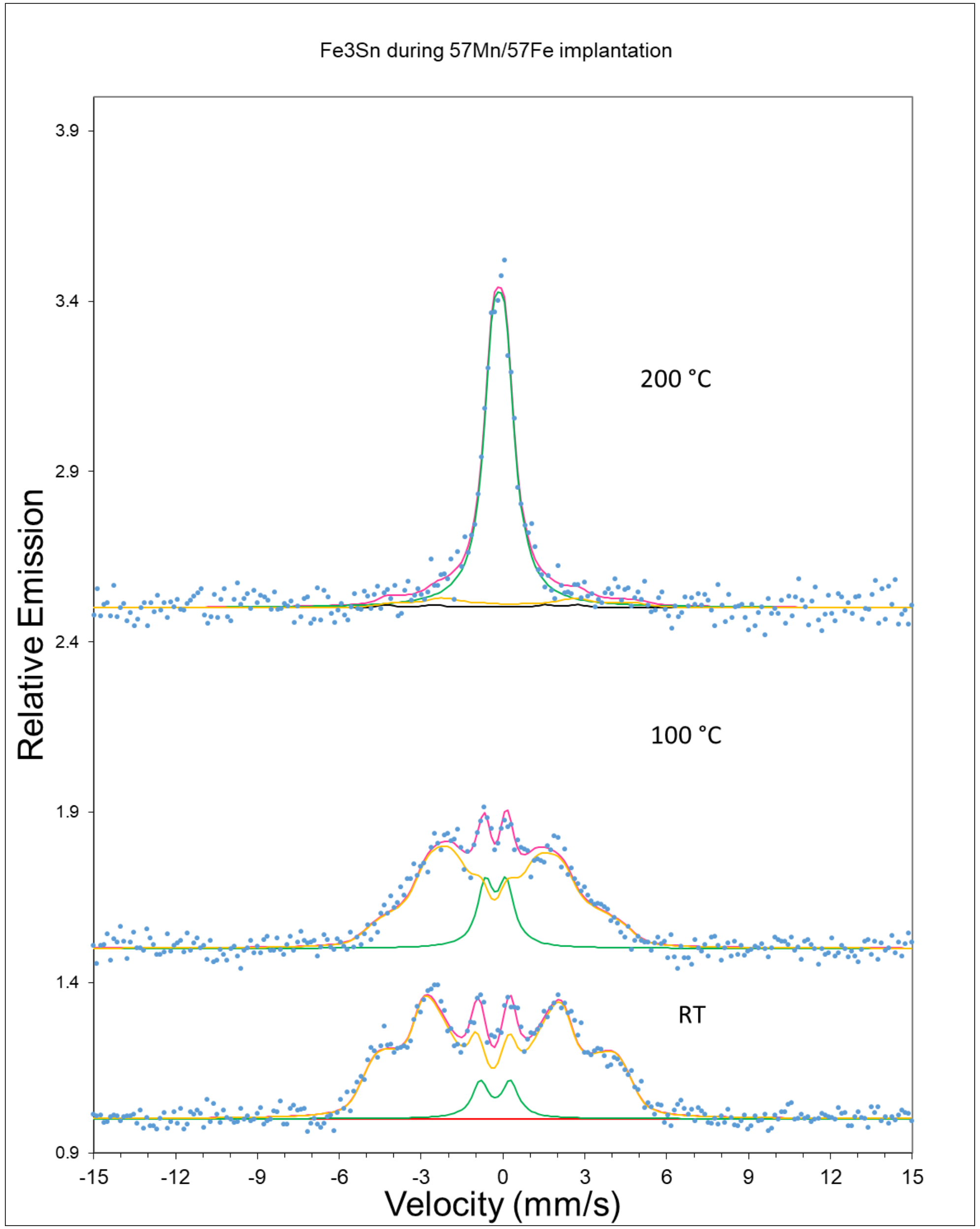

SexGenS			DBL			DIST2			
								B (T)	*f* (relative)
B_{hf} (T)	21.803795					δ_0 (mm/s)	-0.3	33	0
δ (mm/s)	-0.6216704		δ (mm/s)	-0.2837371		δ_1 (mm/s/T)	0	27.560502	-3.1127925
ΔE_Q (mm/s)	-0.2843864		ΔE_Q (mm/s)	1.1048432		$\Delta E_{Q,0}$ (mm/s)	0.15	21	-2.1231911
			Γ (mm/s)	0.7136321		$\Delta E_{Q,1}$ (mm/s/	0	5	0
Outer/middle/inner									
Γ (mm/s)	Area ratio					Γ_{16} (mm/s)	0.6		
0.637776	3					Γ_{25} (mm/s)	0.6		
0.8675067	4					Γ_{34} (mm/s)	0.6		
0.6	1					A_{16}	3		
						A_{25}	2.6842568		
						A_{34}	1		
						Nb	3		
						Average B			
						21.942854			
						Standard dev.			
						6.0573744			
Area (%)	0		Area (%)	8.5005903		Area (%)	91.49941		

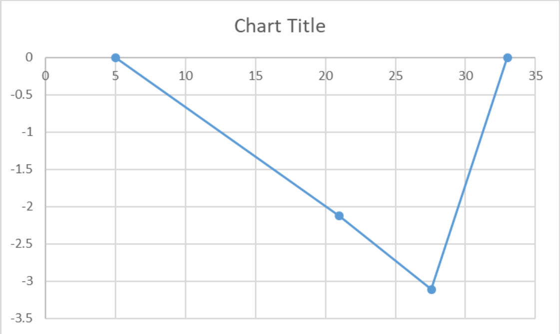

crystals MDPI

Article

Magnetic Structure and Strain State in Fe/V Superlattices Studied by $^{57}Fe^{+}$ Emission and Conversion Electron Mössbauer Spectroscopy

Torben E. Mølholt [1,2], Sveinn Ólafsson [1], Haraldur P. Gunnlaugsson [1], Bingcui Qi [1,*], Karl Johnston [2], Roberto Mantovan [3], Hilary Masenda [4], Krish Bharuth-Ram [5], Hafliði P Gíslason [1], Guido Langouche [6] and Deena Naidoo [4]

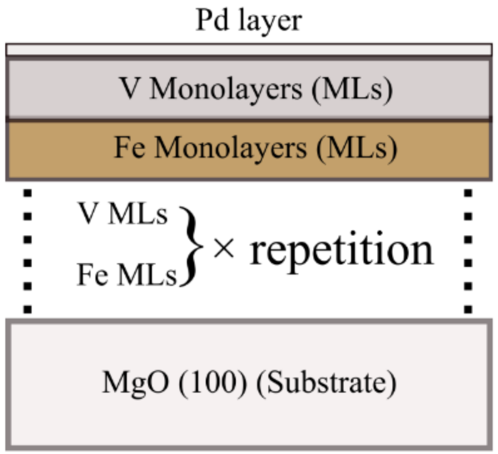

Fe_{Fe} is not fully symmetr
can be described with a
coupling between δ and

$$\delta_{Fe_{Fe}} = \delta_{Fe_{Fe}}(33T) + \delta_1 \times$$

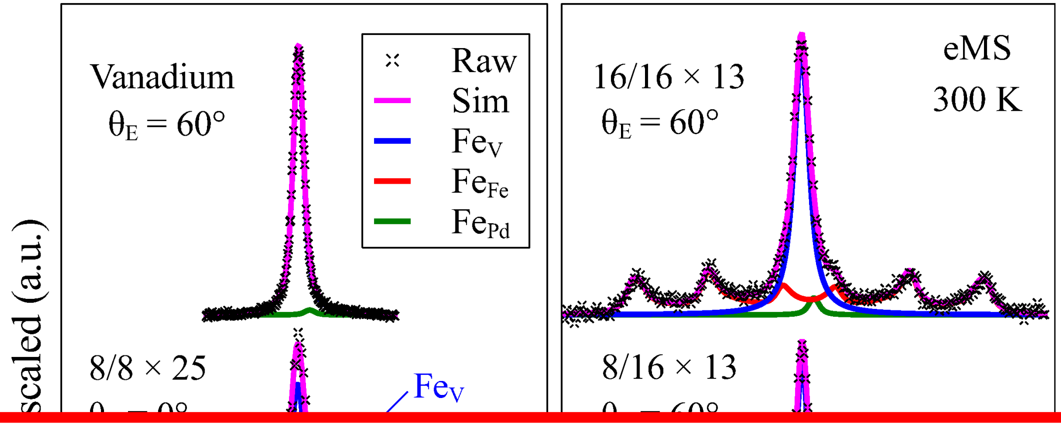

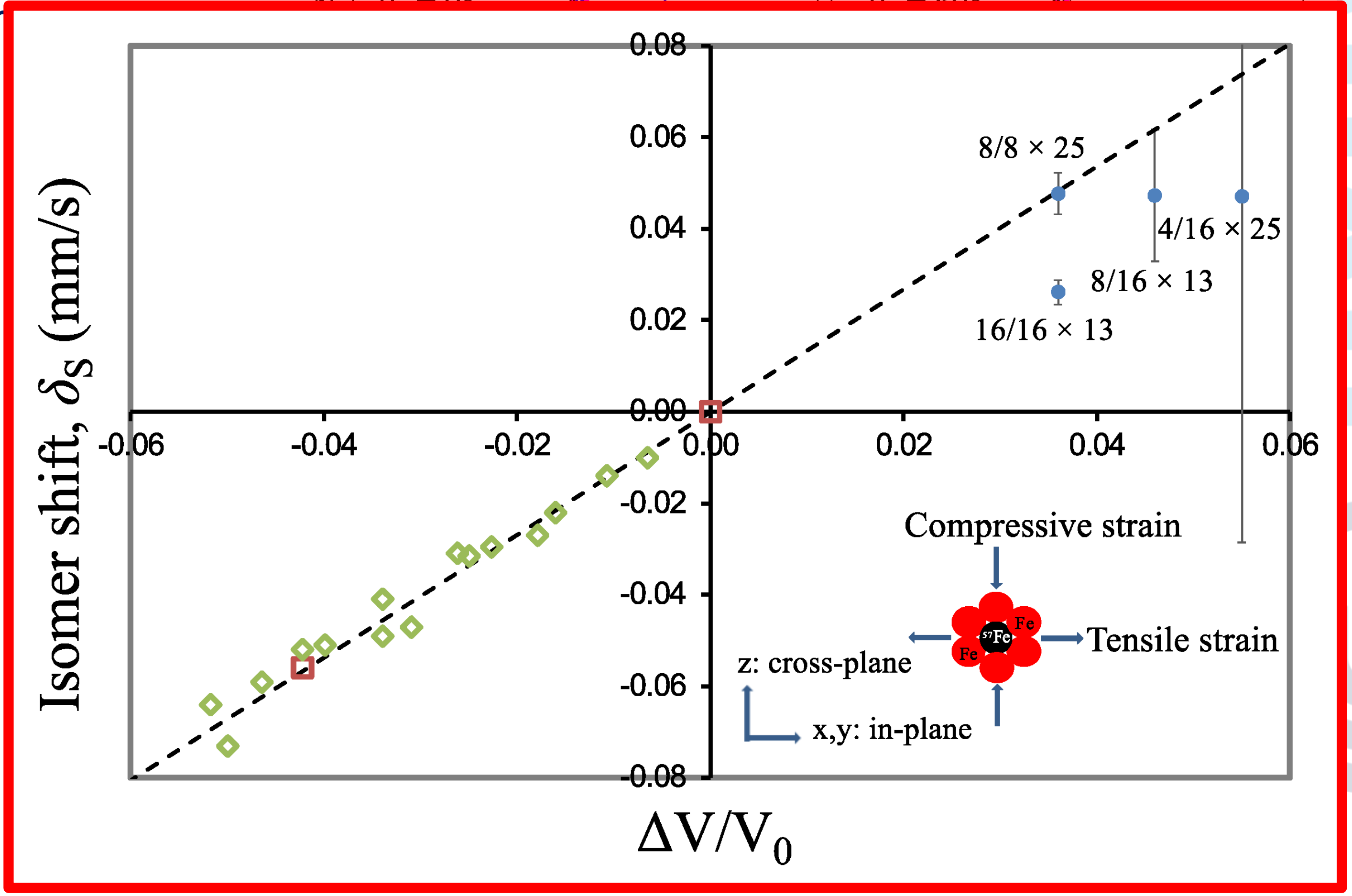

Our study demonstrate that with the online eMS technique the effects of the **strain state** of the superlattice on the magnetic properties of the Fe-layer in the Fe/V multilayer structures **can be detected**

TAC

Emission Mössbauer spectroscopy of topological kagome magnets					
CDS#	**Proposal #**	**IS #**	**Setup**	**Shifts**	**Isotopes**
CERN-INTC-2024-004	INTC-P-687		GLM/GHM	11	57Mn,119In
Beam intensity/purity, targets-ion sources	These isotopes were utilized in numerous SSP runs previously, demonstrating sufficient production yields for the experiment, so no issues are anticipated. *Technical info for future reference:* - *RILIS for 57Mn and 119In -> only indicated for 119In in the proposal but required for both.* - *UCx Ta*				
General implantation and setup					
General Comments					
Safety	ISIEC for this set-up at EDMS 2897524 (eMIL) - to be Released. Additional safety checks (i.e. cryogenics) and electrical inspection to be organised with EP Electrical Safety Officer (5.5 kV) and specific Safety Clearance to be delivered before used of the installation. The template EDMS 2938671 (procedure for the collection) and an IMPACT is to be filled, a dry run oganised, in order to get green light from safety standpoint.				
TAC recommendation	**The TAC does not see any feasibility issues with this proposal.**				

Foreseen activity on samples

The general production term for activity in Bq is given by the formula:	
$A = N\sigma\varphi\left(1 - e^{-\lambda t}\right)$	
Where N is the number of atoms,	
σ is the cross section and	
φ the incident fluence of particles.	
The yield provided in the ISOLDE database is a simplified expression of	
$N\sigma\varphi$	
it provides the number of ions per charge unit of the primary proton beam.	
For example, 3E7 ions per µC means 3E7 ions per second of 1 µA of the primary proton beam.	Updated 119In yield is 3E7 ions per µC
However, if we have full intensity of protons, i.e. 2 µA, we will have 6E7 ions per second.	
When the half-life is short, we reach saturation quickly, meaning that the expression	
$e^{-\lambda t}$	
is close to zero.	
Then with short half-lives, the activity at saturation is equal to the production rate, in this case 6E7 Bq or 60 MBq.	

Ferromagnets

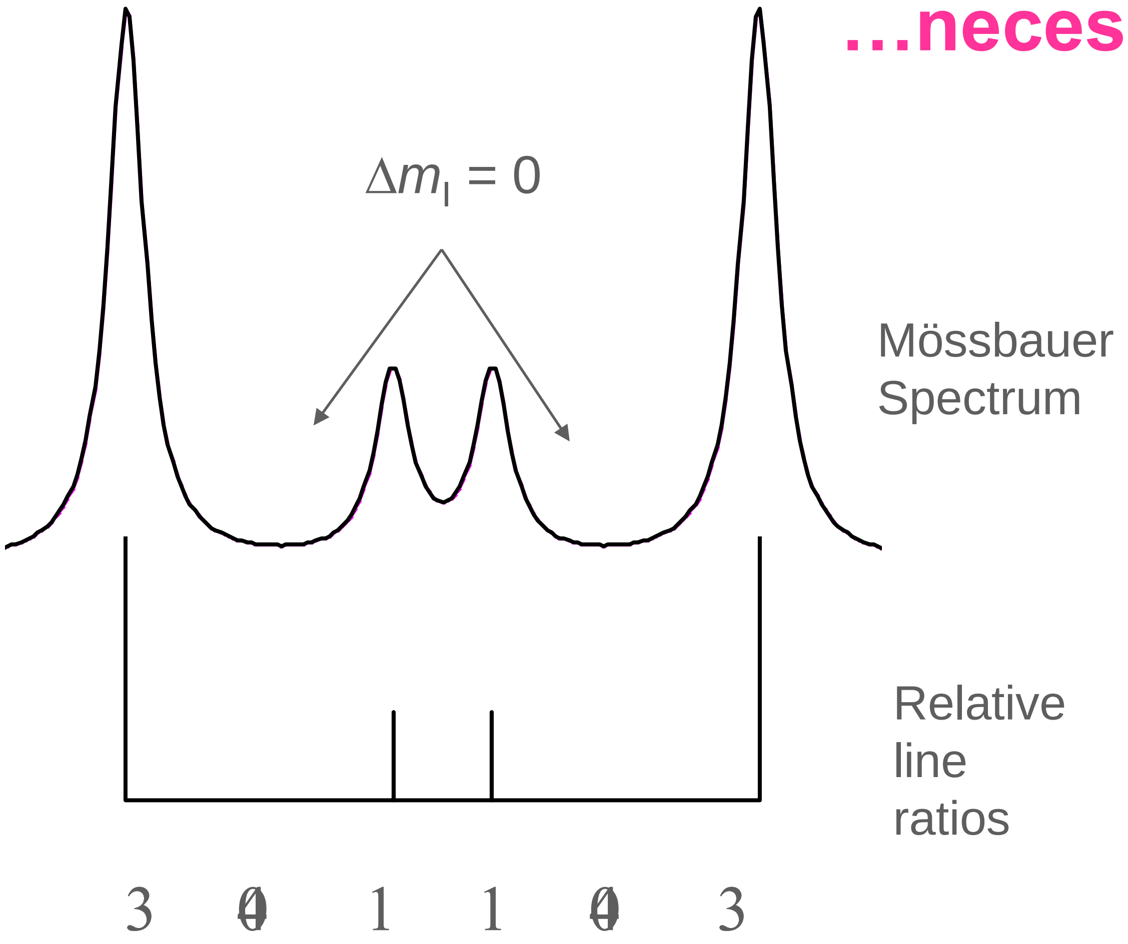

…necessary to apply B_{ext}

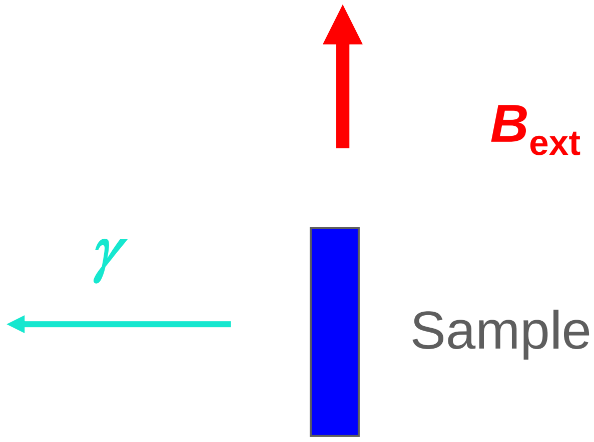

Individual line ratios depend on the angle between B_{ext} and γ

Slowly-relaxing paramagnets

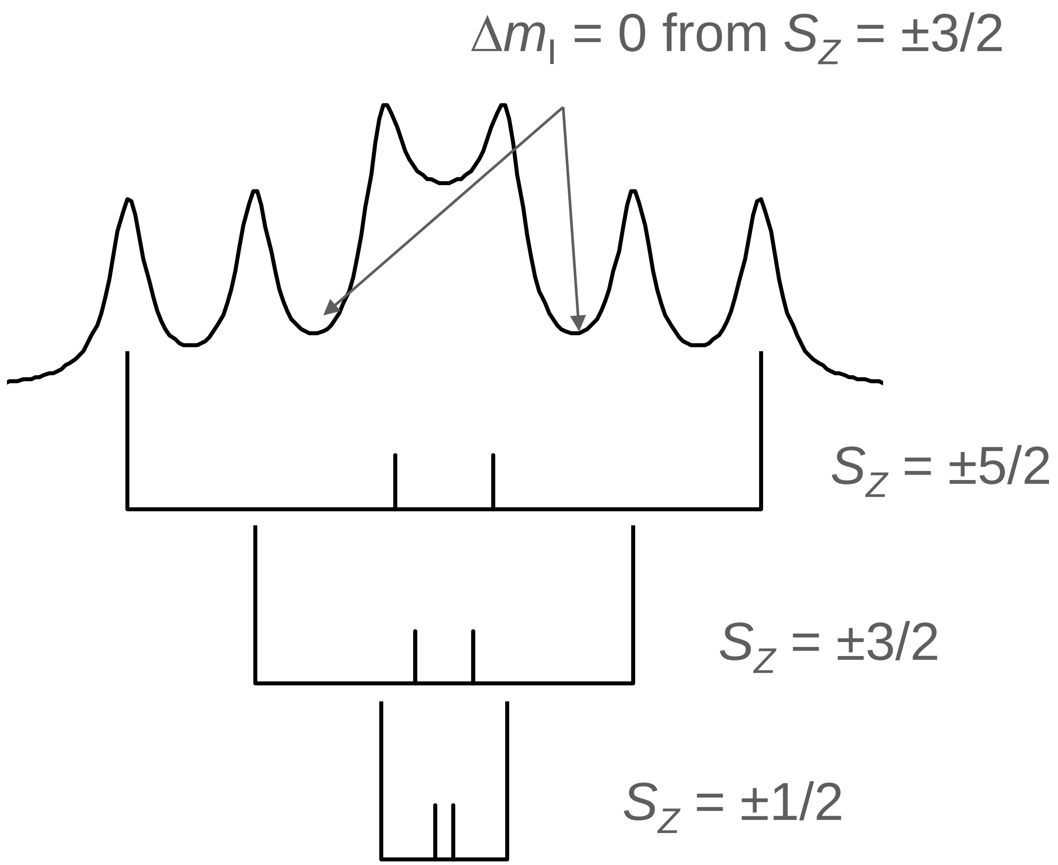

Paramagnetic Fe in a crystal field: Kramers doublets

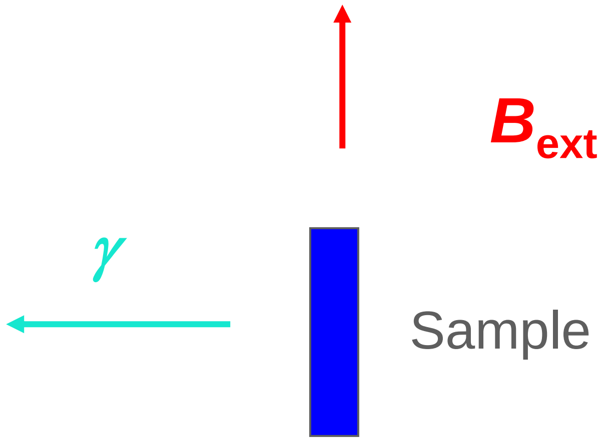

Individual line ratios depend on the angle between B_{ext} and γ

Paramagnetic Fe^{3+} in axially stymmetric crystal field splits into the 3 Kramers doublets $S_Z = \pm 1/2, \pm 3/2, \pm 5/2$

Topological Magnetic Weyl and massive Dirac systems: the Kagome (anti)ferromagnets

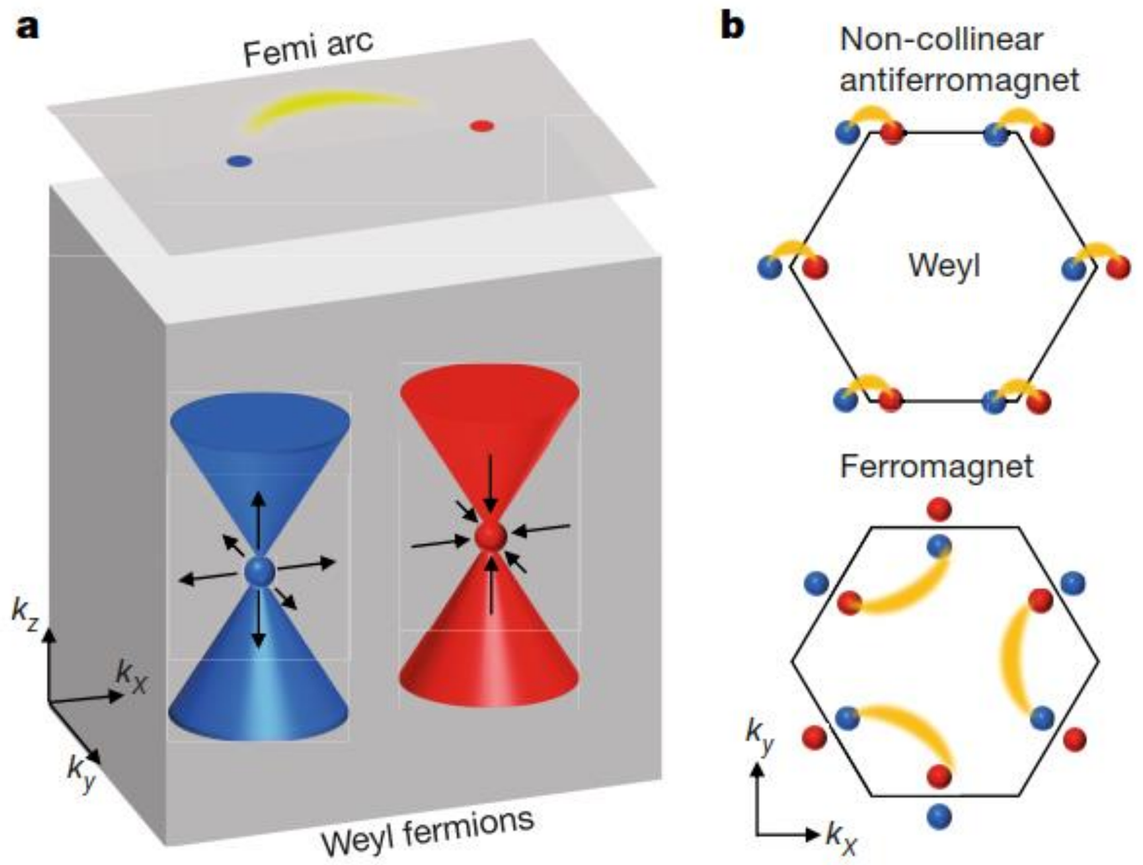

J.-X. Yin, B. Lian & M.Z. Hasan, Nature **612**, 657 (2022).

Illustration of a pair of Weyl fermion quasiparticles with opposite chiral charges (red and blue spheres) in the 3D momentum space. The arrows illustrate the direction of the Berry curvature field in the vicinity of each Weyl fermion. The red and blue cones illustrate their respective linear Weyl dispersions in the bulk momentum space. On the top surface, a Fermi arc state (yellow arc) connects two Weyl cones in the surface momentum space. b, Illustration of Weyl Fermion positions and Fermi arc connectivity in the surface momentum space of the kagome non-collinear antiferromagnet Mn_3Sn (top) and a kagome Ferromagnet, e.g. Fe_3Sn (bottom). Owing to the rotation-symmetry breaking of the non-colinear antiferromagnetism and spin–orbit coupling, the Weyl

Fermion distribution and Fermi arc connectivity also break rotational symmetry.

Ferromagnetic Kagome Fe_3Sn_2 hosts massive Dirac fermions

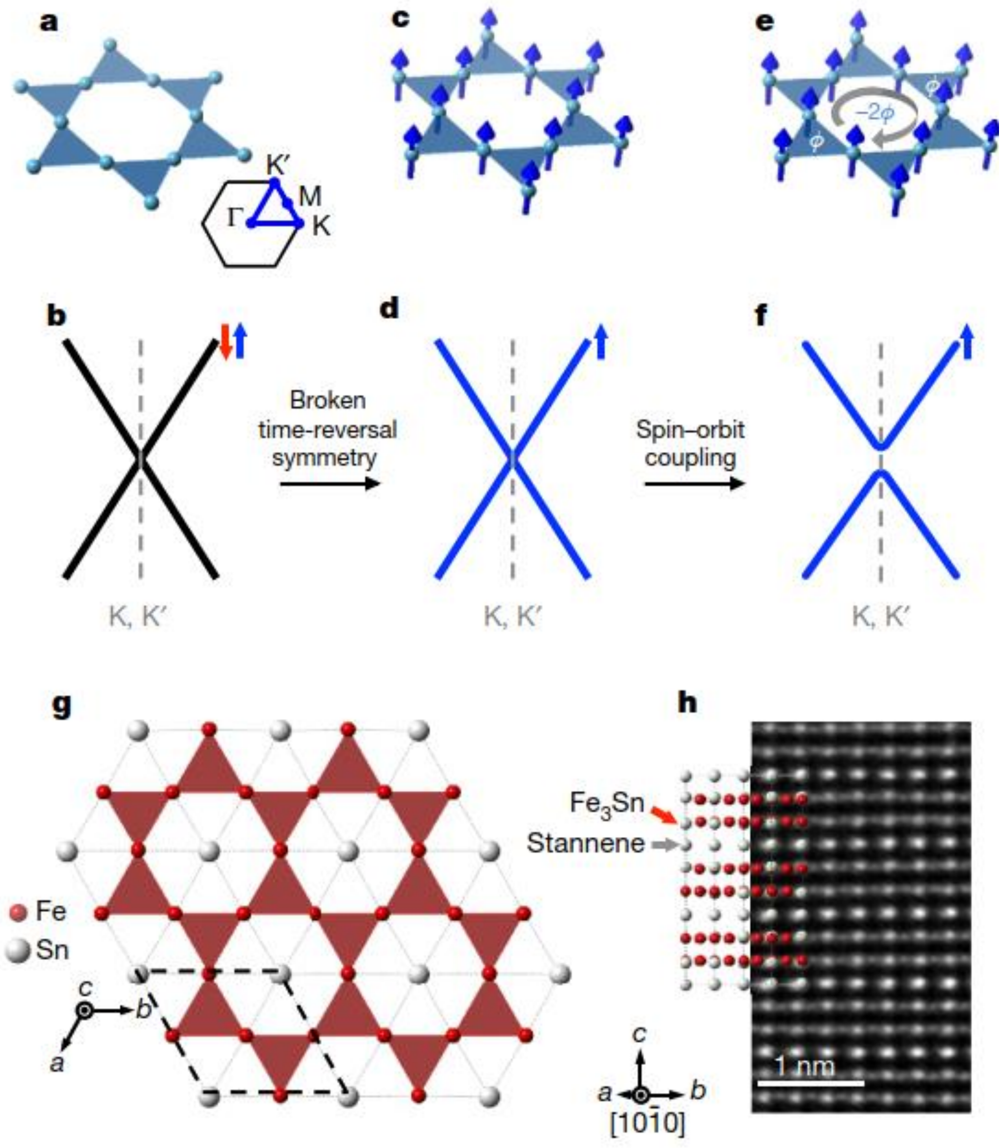

The kagome structure and Fe_3Sn_2. a, b, Structure of the kagome lattice (a) and the associated Dirac point in the nearest-neighbour tight-binding model (b), with the Brillouin zone shown in the inset. The band is degenerate, as denoted with red and blue spins. c, d, Ferromagnetic kagome lattice with broken time-reversal symmetry (moments in blue) (c) and the associated spin-polarized Dirac band with coupling between the magnetization and spin (d). e, f, Spin–orbit-coupled ferromagnetic kagome lattice with Berry phase φ accrued via hopping (e) and the corresponding gapped Dirac spectrum (f). g, The Fe_3Sn kagome plane in Fe_3Sn_2, with the kagome network shown in red. h, Transmission electron microscopy cross-section of Fe_3Sn_2 and the corresponding Fe_3Sn and stanene layers viewed from the [1010] direction.

L. Ye *et al.*, Nature **555**, 638 (2018)

Anomalous Hall effect in Fe_3Sn_2

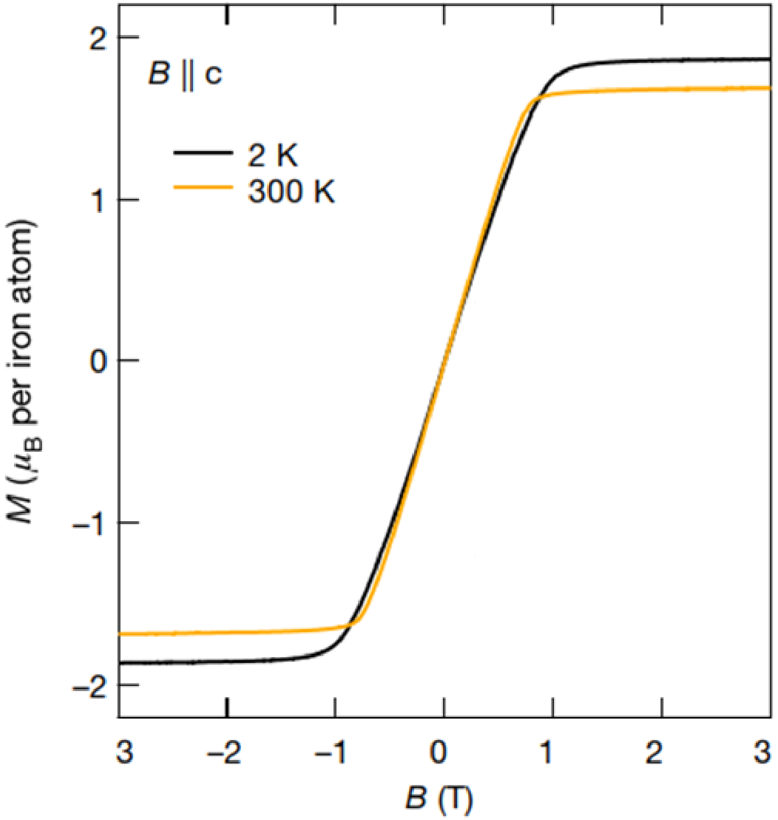

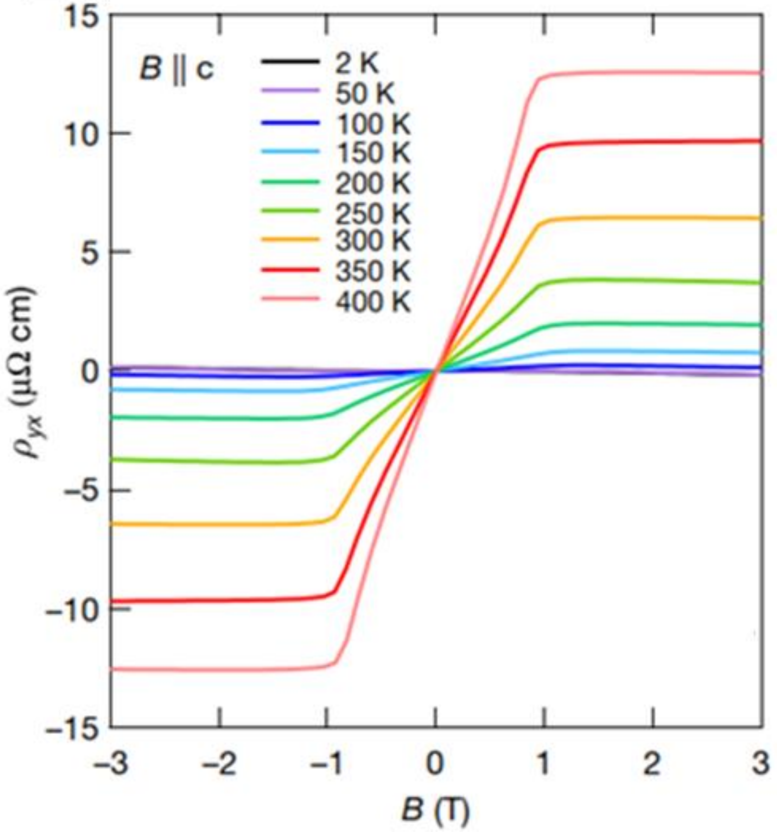

L. Ye *et al.*, Nature **555**, 638 (2018)

Large anomalous Nernst effect in the kagome ferromagnet Fe_3Sn

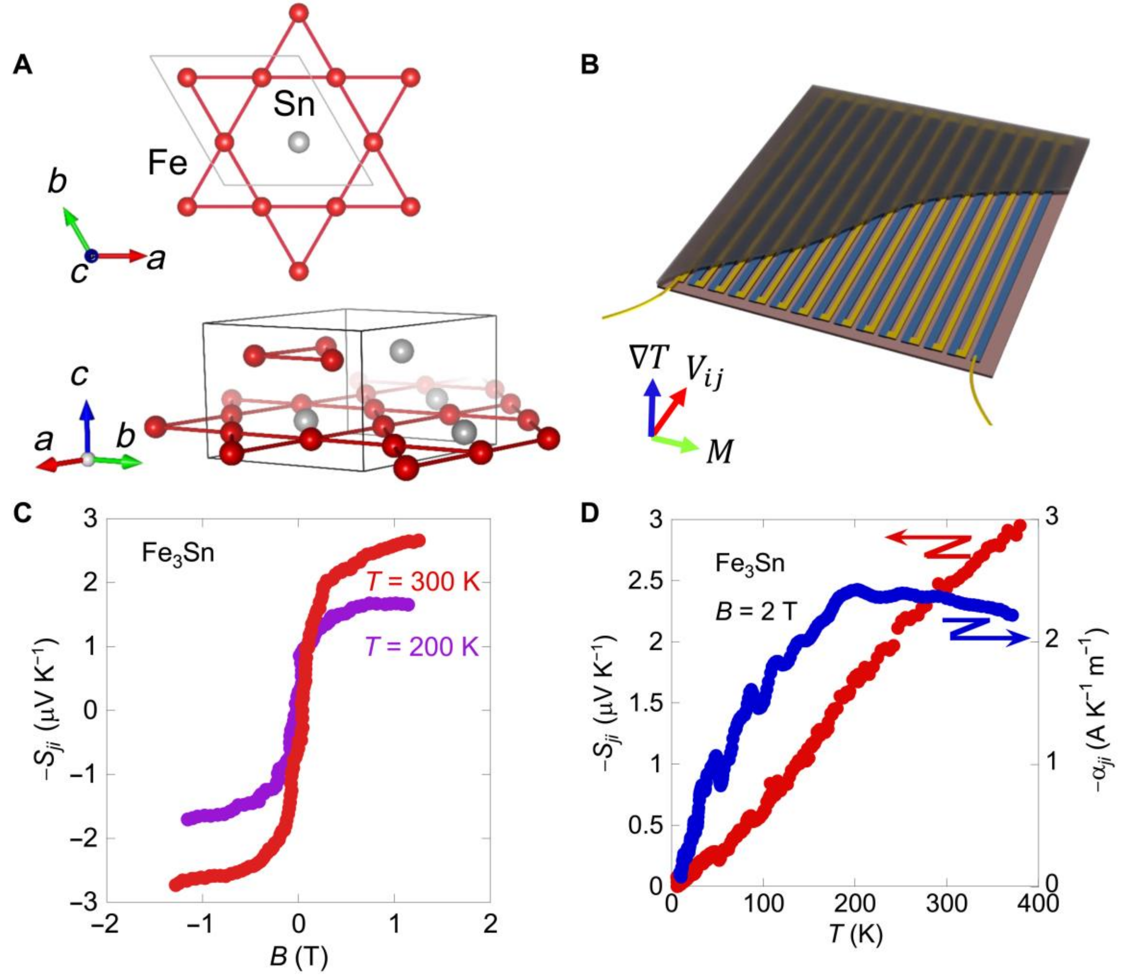

Crystal structure, anomalous Nernst module, ANE, and temperature dependence of ANE of Fe_3Sn.
(**A**) Top view of the kagome lattice of Fe_3Sn with Fe (red) and Sn (gray) atoms, respectively. (**B**) Schematic picture of thermopiles using ANE. (**C**) Nernst coefficient $-S_{ji}$ as a function of magnetic field in polycrystalline Fe_3Sn after the correction of demagnetization effect, reaching up to 2.9 μV K^{-1} at 1 T, 300 K. (**D**) Temperature dependence of the Nernst signal at an external magnetic field of 2 T (red, left axis) and of the transverse thermoelectric conductivity.

T. Chen et al., Sci. Adv. 8, 1480 (2022)

Hexagonal antiferromagnets Mn_3Z (Z = Sn, Ge)

Mn_3Z

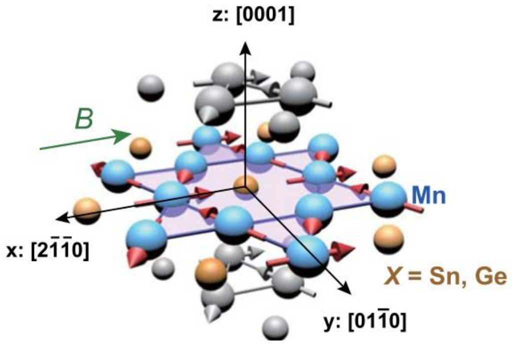

	T_N (K)	Crystal space group
Mn_3Ga[a]	470	$P6_3/mmc$, no. 194
Mn_3Ge[b]	365	
Mn_3Sn[c]	420	

$M_{Mn3Sn} = 3 m\mu_B$ / Mn

$M_{Mn3Ge} = 7 m\mu_B$ / Mn

Zhang *et al*., *Phys. Rev. B* **95**, 075128 (2017)
Tomiyoshi, *Solid Sate Commun.* **42**, 385 (1982)

Mn_3Sn

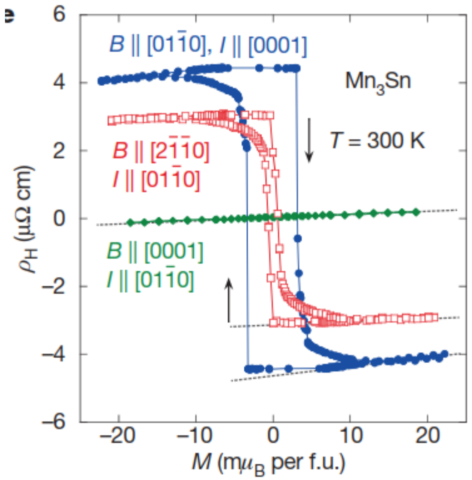

S. Nakatsuji *et al*., *Nature* **527**, 212 (2015)

Mn_3Ge

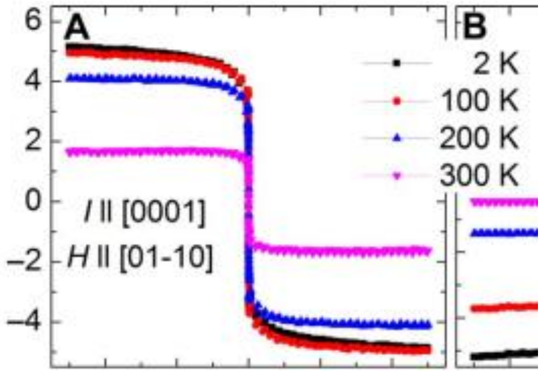

A. K. Nayak *et al*., *Sci. Adv.* **2**, e1501870 (2016)

Magnetic Weyl fermions in Mn_3Sn, a non-collinear antiferromagnet that exhibits a large anomalous Hall effect, even at room temperature.
[K. Kuroda et al., Nat. Mater. 16, 1090 (2017)]

Realization of epitaxial Mn_3Sn noncollinear antiferromagnet at MPI Dresden

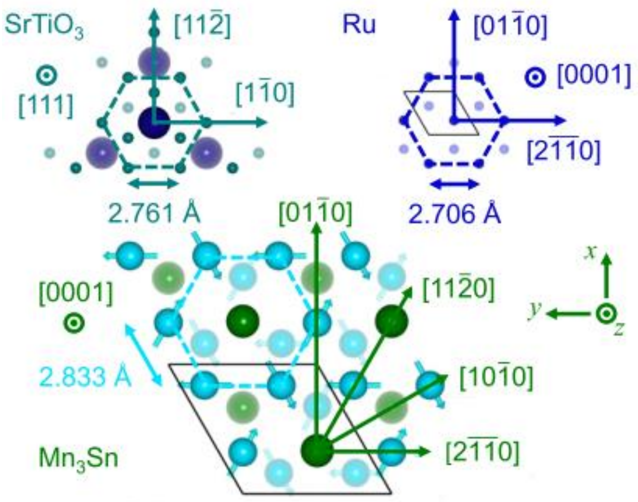

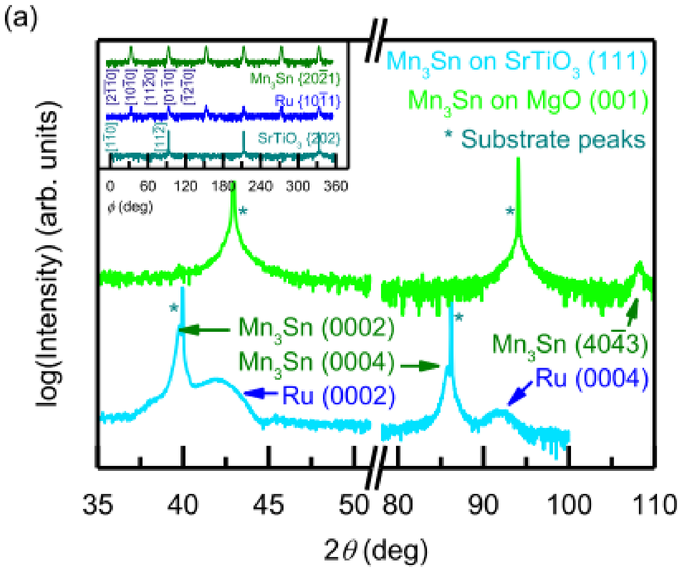

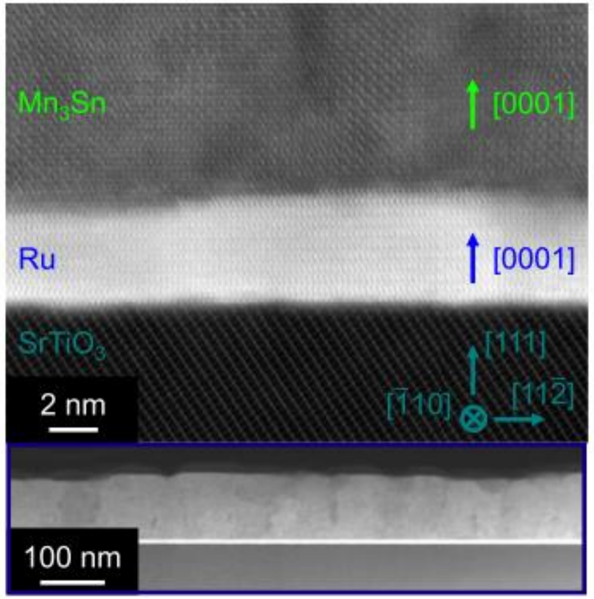

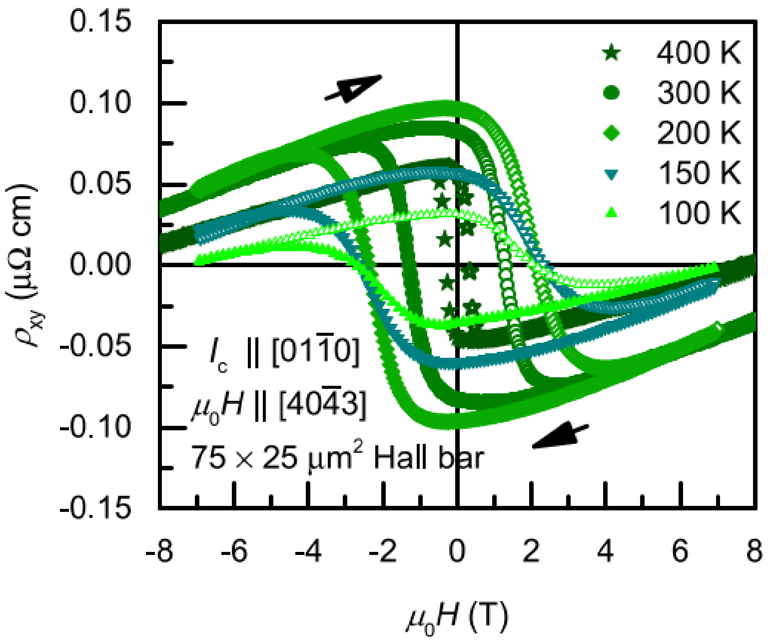

Large anomalous Hall response from momentum-space Berry curvature in an AFM.

[J. Kübler and C. Felser 2014 *EPL* **108** 67001]

James M. Taylor, Anastasios Markou, Edouard Lesne *et al.*, Phys. Rev. B **101**, 094404